EUROPEAN ORGANISATION FOR PARTICLE PHYSICS

CERN-PPE/93-78
May 10, 1993

The Forward-Backward Asymmetry of $e^+e^- \to b\bar{b}$ and $e^+e^- \to c\bar{c}$ Using Leptons in Hadronic Z^0 Decays

The OPAL Collaboration

Abstract

The forward-backward asymmetries of $e^+e^- \to Z^0 \to b\bar{b}$ and $e^+e^- \to Z^0 \to c\bar{c}$ have been measured by the OPAL Collaboration using samples of hadronic Z^0 decays in which electron or muon candidates were observed. The asymmetries were measured simultaneously in a two parameter fit, which used the distributions of the track momentum and transverse momentum component with respect to the associated jet to distinguish lepton candidates from different sources. From a sample of 360 000 hadronic events with centre-of-mass energies within ± 0.5 GeV of the Z^0 mass and mean energy 91.24 GeV, the values obtained for the $b\bar{b}$ asymmetry before and after correcting for the effect of $B^0\overline{B^0}$ mixing, and for the $c\bar{c}$ asymmetry are, respectively:

$$\begin{aligned} A_{FB}^{\mathrm{b,mix}} &= 0.070 \pm 0.014\,(\mathrm{stat}) \pm 0.005\,(\mathrm{sys}), \\ A_{FB}^{\mathrm{b}} &= 0.092 \pm 0.018\,(\mathrm{stat}) \pm 0.007\,(\mathrm{sys}) \pm 0.003\,(\mathrm{mix}), \\ A_{FB}^{\mathrm{c}} &= 0.014 \pm 0.030\,(\mathrm{stat}) \pm 0.020\,(\mathrm{sys}). \end{aligned}$$

The measurement of the $b\bar{b}$ asymmetry is confirmed by a measurement using only leptons with high transverse momentum. This sample is highly enriched in semileptonic decays of b hadrons. Measurements using high transverse momentum leptons were also performed using samples of events with centre-of-mass energies further from the Z^0 mass. After correcting for the effect of $B^0\overline{B^0}$ mixing, the results are:

$$\begin{aligned} A_{FB}^{\mathrm{b}}(\langle\sqrt{s}\rangle = 89.66\,\mathrm{GeV}) &= 0.071 \pm 0.054\,(\mathrm{stat}) \pm 0.007\,(\mathrm{sys}) \pm 0.002\,(\mathrm{mix}), \\ A_{FB}^{\mathrm{b}}(\langle\sqrt{s}\rangle = 92.75\,\mathrm{GeV}) &= 0.131 \pm 0.047\,(\mathrm{stat}) \pm 0.012\,(\mathrm{sys}) \pm 0.004\,(\mathrm{mix}). \end{aligned}$$

(Submitted to Z. Phys. C)

The OPAL Collaboration

P.D. Acton[25], R. Akers[16], G. Alexander[23], J. Allison[16], K.J. Anderson[9], S. Arcelli[2], A. Astbury[28], D. Axen[29], G. Azuelos[18,a], J.T.M. Baines[16], A.H. Ball[17], J. Banks[16], R.J. Barlow[16], S. Barnett[16], R. Bartoldus[3], J.R. Batley[5], G. Beaudoin[18], A. Beck[23], G.A. Beck[13], J. Becker[10], C. Beeston[16], T. Behnke[27], K.W. Bell[20], G. Bella[23], P. Bentkowski[18], P. Berlich[10], S. Bethke[11], O. Biebel[3], I.J. Bloodworth[1], P. Bock[11], B. Boden[3], H.M. Bosch[11], M. Boutemeur[18], H. Breuker[8], P. Bright-Thomas[25], R.M. Brown[20], A. Buijs[8], H.J. Burckhart[8], C. Burgard[27], P. Capiluppi[2], R.K. Carnegie[6], A.A. Carter[13], J.R. Carter[5], C.Y. Chang[17], D.G. Charlton[8], S.L. Chu[4], P.E.L. Clarke[25], J.C. Clayton[1], W.J. Collins[5], I. Cohen[23], J.E. Conboy[15], M. Cooper[22], M. Coupland[14], M. Cuffiani[2], S. Dado[22], G.M. Dallavalle[2], S. De Jong[13], L.A. del Pozo[5], H. Deng[17], A. Dieckmann[11], M. Dittmar[4], M.S. Dixit[7], E. do Couto e Silva[12], J.E. Duboscq[8], E. Duchovni[26], G. Duckeck[11], I.P. Duerdoth[16], D.J.P. Dumas[6], P.A. Elcombe[5], P.G. Estabrooks[6], E. Etzion[23], H.G. Evans[9], F. Fabbri[2], B. Fabbro[21], M. Fierro[2], M. Fincke-Keeler[28], H.M. Fischer[3], D.G. Fong[17], M. Foucher[17], A. Gaidot[21], J.W. Gary[4], J. Gascon[18], N.I. Geddes[20], C. Geich-Gimbel[3], S.W. Gensler[9], F.X. Gentit[21], G. Giacomelli[2], R. Giacomelli[2], V. Gibson[5], W.R. Gibson[13], J.D. Gillies[20], J. Goldberg[22], D.M. Gingrich[30,a], M.J. Goodrick[5], W. Gorn[4], C. Grandi[2], F.C. Grant[5], J. Hagemann[27], G.G. Hanson[12], M. Hansroul[8], C.K. Hargrove[7], P.F. Harrison[13], J. Hart[8], P.M. Hattersley[1], M. Hauschild[8], C.M. Hawkes[8], E. Heflin[4], R.J. Hemingway[6], G. Herten[10], R.D. Heuer[8], J.C. Hill[5], S.J. Hillier[8], T. Hilse[10], D.A. Hinshaw[18], J.D. Hobbs[8], P.R. Hobson[25], D. Hochman[26], R.J. Homer[1], A.K. Honma[28,a], R.E. Hughes-Jones[8], R. Humbert[10], P. Igo-Kemenes[11], H. Ihssen[11], D.C. Imrie[25], A.C. Janissen[6], A. Jawahery[17], P.W. Jeffreys[20], H. Jeremie[18], M. Jimack[1], M. Jones[29], R.W.L. Jones[8], P. Jovanovic[1], C. Jui[4], D. Karlen[6], K. Kawagoe[24], T. Kawamoto[24], R.K. Keeler[28], R.G. Kellogg[17], B.W. Kennedy[15], S. Kluth[5], T. Kobayashi[24], D.S. Koetke[8], T.P. Kokott[3], S. Komamiya[24], L. Köpke[8], J.F. Kral[8], R. Kowalewski[6], J. von Krogh[11], J. Kroll[9], M. Kuwano[24], P. Kyberd[13], G.D. Lafferty[16], H. Lafoux[21], R. Lahmann[17], F. Lamarche[18], J.G. Layter[4], P. Leblanc[18], A.M. Lee[31], M.H. Lehto[15], D. Lellouch[26], C. Leroy[18], J. Letts[4], S. Levegrün[3], L. Levinson[26], S.L. Lloyd[13], F.K. Loebinger[16], J.M. Lorah[17], B. Lorazo[18], M.J. Losty[7], X.C. Lou[12], J. Ludwig[10], A. Luig[10], M. Mannelli[8], S. Marcellini[2], C. Markus[3], A.J. Martin[13], J.P. Martin[18], T. Mashimo[24], P. Mättig[3], U. Maur[3], J. McKenna[28], T.J. McMahon[1], J.R. McNutt[25], F. Meijers[8], D. Menszner[11], F.S. Merritt[9], H. Mes[7], A. Michelini[8], R.P. Middleton[20], G. Mikenberg[26], J. Mildenberger[6], D.J. Miller[15], R. Mir[12], W. Mohr[10], C. Moisan[18], A. Montanari[2], T. Mori[24], M. Morii[24], U. Müller[3], B. Nellen[3], H.H. Nguyen[9], S.W. O'Neale[1], F.G. Oakham[7], F. Odorici[2], H.O. Ogren[12], C.J. Oram[28,a], M.J. Oreglia[9], S. Orito[24], J.P. Pansart[21], B. Panzer-Steindel[8], P. Paschievici[26], G.N. Patrick[20], N. Paz-Jaoshvili[23], M.J. Pearce[1], P. Pfister[10], J.E. Pilcher[9], J. Pinfold[30], D. Pitman[28], D.E. Plane[8], P. Poffenberger[28], B. Poli[2], A. Pouladdej[6], T.W. Pritchard[13], H. Przysiezniak[18], G. Quast[27], M.W. Redmond[8], D.L. Rees[8], G.E. Richards[16], S.A. Robins[13], D. Robinson[8], A. Rollnik[3], J.M. Roney[28,b], E. Ros[8], S. Rossberg[10], A.M. Rossi[2], M. Rosvick[28], P. Routenburg[6], K. Runge[10], O. Runolfsson[8], D.R. Rust[12], M. Sasaki[24], C. Sbarra[2], A.D. Schaile[10], O. Schaile[10], W. Schappert[6], P. Scharff-Hansen[8], P. Schenk[4], B. Schmitt[3], H. von der Schmitt[11], M. Schröder[12], C. Schwick[27], J. Schwiening[3], W.G. Scott[20], M. Settles[12], T.G. Shears[5], B.C. Shen[4], C.H. Shepherd-Themistocleous[7], P. Sherwood[15], R. Shypit[29], G.P. Siroli[2], A. Skillman[16], A. Skuja[17], A.M. Smith[8], T.J. Smith[28], G.A. Snow[17], R. Sobie[28,b], R.W. Springer[17], M. Sproston[20], A. Stahl[3], C. Stegmann[10], K. Stephens[16], J. Steuerer[28], R. Ströhmer[11], D. Strom[19], H. Takeda[24], T. Takeshita[24,c], S. Tarem[26], M. Tecchio[9], P. Teixeira-Dias[11], N. Tesch[3], M.A. Thomson[15], E. Torrente-Lujan[22], S. Towers[28], G. Transtromer[25], N.J. Tresilian[16], T. Tsukamoto[24], M.F. Turner[8], D. Van den plas[18], R. Van Kooten[27], G.J. VanDalen[4], G. Vasseur[21], C.J. Virtue[7], A. Wagner[27], D.L. Wagner[9], C. Wahl[10], C.P. Ward[5], D.R. Ward[5], P.M. Watkins[1], A.T. Watson[1], N.K. Watson[8], M. Weber[11], P. Weber[6], P.S. Wells[8], N. Wermes[3], M.A. Whalley[1], B. Wilkens[10], G.W. Wilson[4], J.A. Wilson[1], V-H. Winterer[10], T. Wlodek[26], G. Wolf[26], S. Wotton[11], T.R. Wyatt[16], R. Yaari[26], A. Yeaman[13], G. Yekutieli[26], M. Yurko[18], W. Zeuner[8], G.T. Zorn[17].

[1]School of Physics and Space Research, University of Birmingham, Birmingham, B15 2TT, UK
[2]Dipartimento di Fisica dell' Università di Bologna and INFN, Bologna, 40126, Italy
[3]Physikalisches Institut, Universität Bonn, D-5300 Bonn 1, Germany
[4]Department of Physics, University of California, Riverside, CA 92521 USA
[5]Cavendish Laboratory, Cambridge, CB3 0HE, UK
[6]Carleton University, Dept of Physics, Colonel By Drive, Ottawa, Ontario K1S 5B6, Canada
[7]Centre for Research in Particle Physics, Carleton University, Ottawa, Ontario K1S 5B6, Canada
[8]CERN, European Organisation for Particle Physics, 1211 Geneva 23, Switzerland
[9]Enrico Fermi Institute and Dept of Physics, University of Chicago, Chicago Illinois 60637, USA
[10]Fakultät für Physik, Albert Ludwigs Universität, D-7800 Freiburg, Germany
[11]Physikalisches Institut, Universität Heidelberg, Heidelberg, Germany
[12]Indiana University, Dept of Physics, Swain Hall West 117, Bloomington, Indiana 47405, USA
[13]Queen Mary and Westfield College, University of London, London, E1 4NS, UK
[14]Birkbeck College, London, WC1E 7HV, UK
[15]University College London, London, WC1E 6BT, UK
[16]Department of Physics, Schuster Laboratory, The University, Manchester, M13 9PL, UK
[17]Department of Physics, University of Maryland, College Park, Maryland 20742, USA
[18]Laboratoire de Physique Nucléaire, Université de Montréal, Montréal, Quebec, H3C 3J7, Canada
[19]University of Oregon, Dept of Physics, Eugene, Oregon 97403, USA
[20]Rutherford Appleton Laboratory, Chilton, Didcot, Oxfordshire, OX11 0QX, UK
[21]DAPNIA/SPP, Saclay, F-91191 Gif-sur-Yvette, France
[22]Department of Physics, Technion-Israel Institute of Technology, Haifa 32000, Israel
[23]Department of Physics and Astronomy, Tel Aviv University, Tel Aviv 69978, Israel
[24]International Centre for Elementary Particle Physics and Dept of Physics, University of Tokyo, Tokyo 113, and Kobe University, Kobe 657, Japan
[25]Brunel University, Uxbridge, Middlesex, UB8 3PH UK
[26]Nuclear Physics Department, Weizmann Institute of Science, Rehovot, 76100, Israel
[27]Universität Hamburg/DESY, II Inst für Experimental Physik, 2000 Hamburg 52, Germany
[28]University of Victoria, Dept of Physics, P O Box 3055, Victoria BC V8W 3P6, Canada
[29]University of British Columbia, Dept of Physics, Vancouver BC V6T 1Z1, Canada
[30]University of Alberta, Dept of Physics, Edmonton AB T6G 2N5, Canada
[31]Duke University, Dept of Physics, Durham, North Carolina 27708-0305, USA

[a]Also at TRIUMF, Vancouver, Canada V6T 2A3
[b]And IPP, University of Victoria, Dept of Physics, P O Box 3055, Victoria BC V8W 3P6, Canada
[c]Also at Shinshu University, Matsumoto 390, Japan

1 Introduction

In the Standard Model, the differential cross-section for the production of fermion-antifermion pairs in e^+e^- annihilation with centre-of-mass energy near to the Z^0 mass can be expressed as:

$$\frac{d\sigma}{d\cos\theta} \propto 1 + \cos^2\theta + \frac{8}{3} A_{FB} \cos\theta, \tag{1}$$

where θ is the angle between the directions of the outgoing fermion and incoming electron, and mass terms have been neglected. This form makes explicit the resulting forward-backward asymmetry, A_{FB}, which in general is defined by $A_{FB} = (\sigma_F - \sigma_B)/(\sigma_F + \sigma_B)$, where σ_F and σ_B are the cross-sections for the fermion to have $\cos\theta > 0$ and $\cos\theta < 0$ respectively. The asymmetry is directly related to the vector, v, and axial-vector, a, couplings of the electron and fermion, f, to the Z^0. At the Z^0 resonance it has the approximate form [1]:

$$A_{FB} \approx \frac{3}{4} \frac{2v_e a_e}{(v_e^2 + a_e^2)} \frac{2v_f a_f}{(v_f^2 + a_f^2)}. \tag{2}$$

To take into account QCD effects, the asymmetry at the parton level can be defined either in terms of the quark direction, or the direction of the thrust axis of the event. The latter is more common, and is used here. The first order QCD correction to the $b\overline{b}$ asymmetry for this definition is a change in the predicted asymmetry of $\delta A_{FB}^{b} = 0.003$ [1].

The measurements presented here use prompt leptons to tag $b\overline{b}$ and $c\overline{c}$ events. Here "prompt" is taken to mean a lepton from a b or c hadron decay. The thrust axis is used to estimate the quark direction, and the quark charge is inferred from the lepton charge. The experimental observable, $y = -Q\cos\theta_{\rm thrust}$, is chosen to estimate $\cos\theta$ for b quarks. Here $\cos\theta_{\rm thrust}$ is the cosine of the angle between the event thrust axis and the incoming electron direction, and Q is the lepton charge. The direction of the thrust axis is chosen so that $\vec{t}.\vec{p}$ is positive, where $\vec{t}$ is the thrust vector, and $\vec{p}$ is the lepton momentum. An event with $y > 0$ ($y < 0$) is said to be forward (backward). The effect of $B^0\overline{B^0}$ mixing is to reduce the apparent asymmetry of $b\overline{b}$ events to $A_{FB}^{b,mix} = (1 - 2\chi)A_{FB}^{b}$ where χ is the average mixing parameter measured using semileptonic b hadron decays produced at Z^0 energies. Events contribute to the overall asymmetry of the sample according to the decaying quark and the semileptonic decay as follows[1]:

- $b \to \ell^-$ with asymmetry $A_{FB}^{b,mix}$
- $b \to \tau^- \to \ell^-$ with asymmetry $A_{FB}^{b,mix}$
- $b \to c \to \ell^+$ with asymmetry $-A_{FB}^{b,mix}$
- $b \to \overline{c} \to \ell^-$ with asymmetry $A_{FB}^{b,mix}$
- $b \to J/\psi \to \ell$ with zero asymmetry
- $c \to \ell^+$ with asymmetry $-A_{FB}^{c}$
- Background from any track wrongly identified as a prompt lepton, with asymmetry A_{FB}^{back}.

The various samples of prompt leptons are characterised by different distributions in momentum, p, and transverse momentum component with respect to the flight direction of the parent hadron, which is approximated by the momentum component, p_t, transverse to the direction of the associated jet. The relatively large mass of the b quark results in hard fragmentation, which leads to a hard momentum spectrum of the produced leptons, and the large momentum of the b hadron decay products

[1]Charge conjugate decay chains are implied. For example, $b \to c \to \ell^+$ also refers to the process $\bar{b} \to \bar{c} \to \ell^-$. The expression $b \to c \to \ell$ refers to the four "cascade" decays: $b \to c \to \ell^+$, $b \to \overline{c} \to \ell^-$ and their charge conjugates.

in the hadron rest frame is manifested as a large p_t in the experimental frame. Leptons produced by the cascade processes, $b \to c \to \ell$, have lower p and p_t, while the direct $c \to \ell^+$ decays again lead to lower p_t, but relatively high momentum.

Two approaches are presented here. Firstly, the asymmetry was measured in the region with high p and p_t, which is dominated by $b \to \ell^-$ decays. This observed asymmetry was corrected for the small contributions from other sources. Secondly, a simultaneous fit was performed for $A_{FB}^{b,mix}$ and A_{FB}^{c} over the full p_t range. In the following sections the OPAL detector, the selection of hadronic Z^0 decays, and the identification of electrons and muons are described. The measurements rely on the modelling of b and c hadron production and semileptonic decay, and on knowledge of the semileptonic branching ratios, which are described in section 3. The measurements of the $b\overline{b}$ and $c\overline{c}$ asymmetries, and the associated systematic uncertainties are presented. Finally, the results are compared with the predictions of the Standard Model.

2 Event selection

2.1 The OPAL detector

The elements of the OPAL detector [2] used in this analysis are described briefly here. Tracking is performed by the central detector, which includes a vertex drift chamber, a large volume jet chamber and "z-chambers" measuring the z coordinate[2] of tracks in the barrel region of the detector. The jet chamber, which has 159 sense wires per sector, also provides measurements of the ionization, dE/dx, of a charged track. The average resolution is 3.5% for 159 samples [3]. The tracking system is surrounded by a coil which maintains a uniform magnetic field of 0.435 T parallel to the beam direction. The momentum resolution in the barrel region, $|\cos\theta| < 0.7$, in the bending plane of the magnetic field, is given by $\sigma_p/p = \sqrt{(0.02)^2 + (0.0018p)^2}$ (p in GeV/c). In the endcap region, the resolution follows a Gluckstern form [4], with an average resolution for leptons from b decays of $\sigma_p/p = 3.9\%$.

Outside the coil is the electromagnetic calorimeter, composed of lead-glass blocks and instrumented with a presampler. The blocks are approximately $10 \times 10\,\mathrm{cm}^2$ in cross section, and the calorimeter is typically 24 radiation lengths deep. There are 9 440 blocks in the barrel region, $|\cos\theta| < 0.82$, with their longitudinal axes pointing roughly towards the interaction region. In the barrel region, the energy resolution is $\sigma_E/E \approx 2.3\%$ for $E \approx 45$ GeV, measured using $e^+e^- \to e^+e^-$ events. The resolution of the energy divided by the momentum for electrons with E between 2 and 3 GeV is measured to be $\sigma(E/p) \approx 10.5\%$ using $e^+e^- \to e^+e^-\gamma$ events. These resolutions include the effect of the material in front of the calorimeter, which amounts to about $2.1/\sin\theta$ radiation lengths. Each of the two endcap calorimeters, covering $0.81 < |\cos\theta| < 0.98$, consists of 1132 blocks with their long axes parallel to the beam direction. This non-projective geometry presents typically three blocks in the direct line-of-flight of a particle originating from the event vertex and thus yields a crude longitudinal shower sampling. The energy resolution of the endcap calorimeters has been measured to be $\sigma_E/E \approx 4.9\%$ for $E \approx 45$ GeV and $\sigma_E/E \approx 12\%$ for $E \approx 3$ GeV.

The return yoke of the magnet is instrumented with streamer tubes as a hadron calorimeter, and outside it lie muon detectors. There are at least 7, and in most regions 8, absorption lengths of material between the interaction point and the muon detectors. Muons with momenta above 3 GeV/c usually penetrate to the muon chambers. The muon barrel detector covers the region $|\cos\theta| < 0.7$. It is composed of four layers of planar drift chambers, with cylindrical geometry. These give a position accuracy of 1.5 mm in r–ϕ and 2 mm in z. The muon endcap detector covers the polar angle range $0.67 < |\cos\theta| < 0.98$. It is composed of two planes of limited streamer tube arrays at each end of the detector, yielding resolutions of 1–3 mm on the x and y coordinates. The z coordinate is known from

[2] The coordinate system is defined with positive z along the e^- beam direction, and θ and ϕ being the polar and azimuthal angles. The positive x direction points towards the centre of the LEP ring. The origin is taken to be the centre of the OPAL detector.

the surveyed positions of the chambers. The two muon detector subsystems cover 93% of the full solid angle.

2.2 Monte Carlo samples

The JETSET 7.3 Monte Carlo program [5] was used to generate event samples, together with a program to simulate the response of the OPAL detector [6]. Simulated events were processed through the same reconstruction and selection algorithms as data from the detector. The Monte Carlo events were all generated with a centre-of-mass energy of 91.175 GeV. A sample of hadronic Z^0 decays containing the mixture of primary quark flavours predicted by the Standard Model was used to study lepton identification and to evaluate non-prompt backgrounds such as hadrons misidentified as muons or photon conversions. The Lund symmetric fragmentation function [5] was used to describe the hadronization properties of all quark flavours in this sample. These studies are described in sections 2.4 and 2.5. Samples of $b\overline{b}$ and $c\overline{c}$ events, where the fragmentation of the b quarks was described by the fragmentation function of Peterson *et al.* [7], were also generated. The Peterson fragmentation function is expected to give a more realistic description of heavy quark fragmentation than the LUND symmetric scheme. The values of the parameters controlling the Peterson fragmentation function used for $b\overline{b}$ and $c\overline{c}$ events were $\epsilon_b = 0.0055$ and $\epsilon_c = 0.05$ respectively, corresponding to LEP average values of $\langle x_E \rangle_b = 0.70$ and $\langle x_E \rangle_c = 0.51$ [8, 9].

2.3 Selection of hadronic Z^0 decays

This analysis is based on data samples collected during 1990 and 1991, with centre-of-mass energies, $\sqrt{s}$, within ± 3 GeV of the Z^0 mass, M_Z. Hadronic Z^0 events were selected using an algorithm which has been described elsewhere [10]. It was additionally demanded that there be at least seven charged tracks which pass minimal quality requirements in each event. This extra condition reduces the background, in particular Z^0 decays to tau pairs, to a negligible level.

Charged tracks and electromagnetic calorimeter energy clusters not associated to tracks were combined into jets using the JADE algorithm [11], with the E0 recombination scheme [12]. An invariant mass-squared cut-off of $x_{\min} = (7\,\mathrm{GeV}/c^2)^2$ was used. According to Monte Carlo simulation, this jet definition optimises the estimate of the direction of the decaying b hadron. The lepton was included in the calculation of the jet direction for the determination of the transverse momentum, p_t. The same tracks and clusters were also used to find the thrust axis of the event. As the asymmetry measurement relies on the thrust axis to estimate the quark direction, an additional restriction of $|\cos\theta_{\mathrm{thrust}}| < 0.9$ was introduced to ensure that the thrust axis was not biassed by the loss of particles outside the detector acceptance. Similarly, the polar angle of the jet direction was required to satisfy $|\cos\theta_{\mathrm{jet}}| < 0.9$ to ensure that the p_t of the lepton was well measured.

The predicted quark asymmetries depend strongly on the centre-of-mass energy. The data were therefore divided into three samples: (1) events with $\sqrt{s}$ within 0.5 GeV of M_Z, amounting to about 360k events with mean centre-of-mass energy $\langle\sqrt{s}\rangle = 91.24$ GeV, referred to as "on-peak" data; (2) events with $\sqrt{s}$ above this range – 55k events with $\langle\sqrt{s}\rangle = 92.75$ GeV; (3) events with $\sqrt{s}$ below the range of sample (1) – 46k events with $\langle\sqrt{s}\rangle = 89.66$ GeV. Samples (2) and (3) will be referred to collectively as "off-peak" data.

2.4 Muon identification

Tracks in the central detector with polar angle $|\cos\theta| < 0.9$, and momentum $p > 3$ GeV/c were considered as muon candidates. The muon identification criteria were the same as those described in a previous publication [13], in which only muon candidates with $p_t > 1.1$ GeV/c were considered. In this analysis the full p_t range was used, and one extra cut was therefore introduced to reduce the large background at low p_t, as described below. In addition, possible systematic errors due to incorrect

modelling of the shape of the background as a function of p and p_t were considered. The asymmetry measurement does not require a knowledge of the identification efficiency, although in order to check that the events follow the distribution predicted by equation (1) the efficiency as a function of $\cos\theta$ is needed. This is explained in section 4.

Selection criteria

The most effective variable used for muon identification in OPAL measures the goodness of the match between the extrapolation of a charged track reconstructed in the central detector and a track segment reconstructed independently in the muon chambers [13]. The points of closest approach of each extrapolated central track to muon segments are determined. The separation in azimuthal and polar angle between these points and the muon segments is found, and the sum in quadrature of these angular deviations, normalized by their errors, is calculated. The resulting matching measure, $\chi_{\rm pos}$, was required to satisfy:

- $\chi_{\rm pos} < 3.0$.

Further requirements were imposed to suppress backgrounds:

- A track with a reliable measurement of the $\mathrm{d}E/\mathrm{d}x$ in the jet chamber was rejected if the measured ionization was more than two standard deviations below that expected for a muon.
- No more than 20 muon segments were allowed in an azimuthal slice of 300 mrad around a track.
- The second best matching track to a muon segment was required to be at least twice as far in angle from the segment as the best matching track ("misassociation cut").

The $\mathrm{d}E/\mathrm{d}x$ requirement removes mostly $\mathrm{K}^{\pm}$ tracks matched to muon segments, as the ionization losses of muon and charged pion tracks are not sufficiently separated for momenta above 2 GeV/c to offer significant pion rejection. The cut on the number of muon segments reduces background caused by hadronic showers leaking out of the back of the calorimeter. The last cut on the relative matching of the first and second best matched tracks is effective against tracks wrongly associated to muon segments. Such misassociation background dominates at low p_t, and the misassociation cut was therefore not needed for the asymmetry measurement using only high p_t muons.

Muon identification efficiency

The muon reconstruction and matching efficiencies as a function of $\cos\theta$ were measured with muon pair events from two-photon scattering processes, and Z^0 decays. The difference in efficiency between these isolated muons and muons in hadronic Z^0 decays was studied using Monte Carlo events. The efficiency of the $\mathrm{d}E/\mathrm{d}x$ cut in denser track environments was studied using pure samples of known particle types, for example pions from K^0 decays [13]. The muon identification efficiency was found to be reliably simulated by the Monte Carlo program for muons with momenta above 3 GeV/c. For example, the muon identification efficiency in the kinematic region $p > 3$ GeV/c, $p_t > 1.0\,$GeV/c was $76\pm3\%$, where the error is systematic.

Muon backgrounds

There are three main backgrounds to the prompt muon signal [13], which are together referred to as hadronic background. These originate from:

- the decays-in-flight of light hadrons, particularly $\pi^{\pm}$ and $\mathrm{K}^{\pm}$,
- leakage of hadronic interaction products through to the muon detectors ("punchthrough"), and hadrons which do not interact inelastically in the detector material ("sailthrough"),

- random incorrect association of a charged track with a reconstructed muon segment caused by some other particle ("misassociation").

The background level was studied using various samples of identified hadrons, and samples with low prompt muon content. These were selected in data and simulated events using the same algorithms. Identified $K^0 \to \pi^+\pi^-$ decays were used for studying the background from charged pions, complemented by $\tau \to 3\pi$ decays in $Z^0 \to \tau^+\tau^-$ events. Samples of tracks passing some, but not all, of the muon identification requirements were also examined. The tests indicated that the backgrounds from pion and kaon decays in flight can be constrained to an accuracy of $\pm 10\%$, and misassociation to $\pm 25\%$. A $\pm 50\%$ error was assigned to the punchthrough background since it predominates only at very high momenta where fewer tracks were available, and depends on the detailed modelling of the hadronic shower development in the detector material. The overall background rate is understood to within $\pm 13\%$.

The background rate as a function of p, p_t and $y = -Q\cos\theta_{\rm thrust}$ was calculated by measuring the probability that a charged track in a Monte Carlo event gives a hadronic background muon candidate ("fake probability"), and multiplying by the total number of tracks seen in the data in the same kinematic region. This procedure reduces dependence on the fidelity of Monte Carlo modelling of the p and p_t distributions. The fake probability per track is expected to be independent of Q, and was taken to be a symmetric function of y in order to improve the statistical precision. However, the total number of tracks as a function of y is not symmetric, and the background predicted in this way has the same asymmetry as the sample of all tracks in the same kinematic region. The average fake probability per charged track for $p > 3$ GeV/c and $p_t > 1.0$ GeV/c was found to be $(0.47 \pm 0.01\,(\text{stat}))\%$. It varies between 0.6% at low momentum to 0.3% at high momentum and is roughly constant with p_t. The rates for the three background components were varied separately in order to estimate the error due to the uncertainty in the background rate as a function of p and p_t. The modelling of the relative yields of $\pi^\pm$ and $K^\pm$ by the Monte Carlo is not expected to be a significant source of error for the asymmetry measurement, because after the dE/dx cut the fake probabilities per track for the two particle types are the same to within $\pm 30\%$. The distribution of background as a function of $-Q\cos\theta$ is therefore expected to have the same asymmetry as the distribution for all tracks. The relatively small fraction of proton tracks means that sensitivity to modelling of their yield is not expected to be a significant source of error.

2.5 Electron identification

Electron candidates with $p > 2$ GeV/c were selected in both the barrel region of the detector, with $|\cos\theta| < 0.7$, and the endcap region, with $0.815 < |\cos\theta| < 0.91$. The electron selection criteria for the barrel region have been discussed in detail elsewhere [14, 13]. The identification of electrons in the endcap region is particularly important for the measurement of the asymmetry, as this is the region where the greatest difference between the number of forward and backward events is expected.

Selection criteria

Identification of electrons in both regions relies on the specific ionization loss of a track in the jet chamber, dE/dx, and the amount and distribution of energy in the electromagnetic calorimeter around the extrapolated track. The dE/dx requirements are similar in the barrel and endcap regions, while the calorimetric requirements are dictated by the somewhat different geometry of the detector in the two parts.

Electron candidate tracks were required to have a well-determined polar angle, to improve the matching to clusters in the calorimeter. In the barrel region it was demanded that the track fit included at least three space points from the z-chambers, and in the endcap region the track was required to have been successfully constrained to the z coordinate of the end of the last wire encountered by the track before exiting the jet chamber.

The ionization loss in the jet chamber was required to be consistent with that expected for an electron:

- $N^{\sigma}_{\mathrm{d}E/\mathrm{d}x} = [\mathrm{d}E/\mathrm{d}x - (\mathrm{d}E/\mathrm{d}x)_0]/\sigma(\mathrm{d}E/\mathrm{d}x) > -2.0$,

$N^{\sigma}_{\mathrm{d}E/\mathrm{d}x}$ is the difference between the measured ionization loss and the mean $\mathrm{d}E/\mathrm{d}x$ expected for electrons, divided by the expected error. The mean electron $\mathrm{d}E/\mathrm{d}x$ and resolution were determined separately for the barrel and endcap regions. In order to accept only tracks for which $\mathrm{d}E/\mathrm{d}x$ was well measured, the number of samples, N_{samp}, used for the $\mathrm{d}E/\mathrm{d}x$ determination of was required to satisfy:

- $N_{\mathrm{samp}} \geq 40$ (barrel) or 20 (endcap)

In the endcap region, electron candidates were additionally required to satisfy

- $N_{\mathrm{samp}}/N_{\mathrm{CJhit}} > 0.5$,

where N_{CJhit} is the number of hits in the central jet chamber used in the r–ϕ track fit. This requirement discriminates against tracks for which a large number of $\mathrm{d}E/\mathrm{d}x$ samples were discarded due to surrounding track activity. It also results in a more uniform efficiency as a function of $|\cos\theta|$. After these two requirements on the number of $\mathrm{d}E/\mathrm{d}x$ samples, more than 90% of prompt electron candidates in the endcap region have N_{samp} greater than 40.

An electron candidate track was required to be extrapolated to a cluster in the electromagnetic calorimeter. The calorimetric requirements in the barrel region were as follows:

- $N_{\mathrm{pres}} > \min(2.5 + p/2, 10)$ (p in GeV/c);
- $E_{\mathrm{cone}}/(E_{\mathrm{cone}} + \Delta E) > 0.85$ or $\Delta E < 2$ GeV ("lateral spread cut");
- $0.7 < E_{\mathrm{cone}}/p < 1.4$.

A presampler cluster amplitude, N_{pres}, of 2.0 corresponds to the signal due to a beam energy muon. E_{cone} is the total energy deposited in the blocks in the electromagnetic cluster associated with the track whose centres are within 30 mrad of the extrapolated track position at the front face of the lead glass. $E_{\mathrm{cone}} + \Delta E$ is the total energy in this cone plus adjacent blocks[3]. The energies were corrected for energy loss in the material traversed before entering the lead glass.

The calorimetric requirements for the endcap region were as follows:

- $N_{\mathrm{blocks}} < 16$.

This requirement on the number of blocks in the cluster, N_{blocks}, serves mostly to reduce hadronic background in the region $p > 10$ GeV/c, where large overlaps between clusters can artificially raise the measured energy, allowing a hadron to pass a cut on E/p.

Due to the non-projective geometry of blocks in the endcap electromagnetic calorimeter, any energy deposit has a reconstructed centre of gravity in θ which is displaced from the track impact point. This displacement was corrected for each cluster assuming that the cluster was created by an electron originating from the event vertex. Figure 1 shows the difference after correction between the θ values of the track and the cluster, $|\theta_{\mathrm{track}} - \theta_{\mathrm{cluster}}|$, which is small for electrons, and broad for hadrons. Electron candidates were required to satisfy:

- $|\theta_{\mathrm{track}} - \theta_{\mathrm{cluster}}| < 8$ mrad.

To reduce further the effect of overlapping clusters on the energy measurement, a background subtracted energy was calculated. Each candidate track was extrapolated to the electromagnetic calorimeter to find the first block through which the track would traverse 4 radiation lengths of material (centre

[3]In a previous publication [14] the variable E_{cone2} was used to represent $E_{\mathrm{cone}} + \Delta E$.

block). Around this centre block, two rings of neighbouring blocks were formed (see figure 2). The inner ring consisted of the 8 blocks touching the centre block, and the outer ring of the 16 next-to-touching blocks. The energies in 11 blocks in the outer ring, excluding the 5 most forward blocks with respect to the track momentum vector in the x–y plane, were averaged. These blocks were chosen as being least affected by energy deposited by the electron candidate itself and typical of the surrounding hadronic activity. This average was subtracted from the centre and each of the 8 touching blocks. Finally, the adjusted energies of the 9 inner blocks were summed and the total was corrected for the energy lost in the material before the calorimeter and for the incidence angle. The ratio between this background subtracted energy, $E_{\rm sub}$, and the momentum was required to satisfy:

- $0.8 < E_{\rm sub}/p < 1.2$.

As well as reducing the effect of overlapping clusters on the energy measurement, the background subtracted energy improves the discrimination between electrons and hadrons. In figure 3, it can be seen that pions are moved out of the signal region after subtracting the estimated energy due to nearby particles.

Photon conversion rejection

Electron candidate tracks tagged as originating from photon conversions were removed from the sample. Photon conversions were identified using an algorithm that searches for pairs of oppositely-charged tracks with a vertex geometry consistent with that expected from a conversion [13]. The efficiency of this conversion tagging method was determined using simulated events and was found to be $(84 \pm 4)\%$ for tracks with $p > 2$ GeV/c and $p_t > 0.8$ GeV/c. This efficiency depends only weakly on p, p_t and θ. The error is systematic and arises from tracking and detector modelling uncertainties. The purity of the tagged conversion sample obtained this way is $(70 \pm 10)\%$ for $p_t > 0.8$ GeV/c.

Hadrons misidentified as electrons

The independence of the E/p and $\mathrm{d}E/\mathrm{d}x$ measurements was used to determine the number of hadrons which were misidentified as electrons, following the procedure described in detail elsewhere [14,13]. The shape of the hadronic background in the E/p distribution was predicted using a sample of tracks which satisfied all the other electron identification criteria, with the $\mathrm{d}E/\mathrm{d}x$ requirement modified to select background tracks. Similarly, the shape of the background in the $\mathrm{d}E/\mathrm{d}x$ distribution was predicted using a modified E/p requirement. The fraction of the sample arising from hadrons misidentified as electrons varies with p and p_t. For $p > 2$ GeV/c and $p_t > 0.8$ GeV/c it is $(3.6 \pm 0.3)\%$. The fraction is at most about 25%, for $p > 6$ GeV/c and $p_t < 0.4$ GeV/c.

Electron identification efficiencies

The electron identification efficiencies and background fractions were calculated using the methods described elsewhere [14, 13]. The efficiency for a prompt electron to satisfy the selection criteria is approximately 45% for $p_t > 0.8$ GeV/c, depending on the momentum region. Although the average electron identification efficiency does not need to be known in order to measure the asymmetry, the relative efficiencies for electrons from different sources must be known. The variation of identification efficiency with $\cos\theta$ can be used to verify the form of equation (1), as described in section 4.

The electron identification efficiency is expected to depend on the source of the prompt electron because the values of some selection variables depend on the density of particles around the electron. The Monte Carlo simulation suggests that the dominant contributions to the variation of efficiency with source are from the lateral spread cut for electrons in the barrel region, and the $E_{\rm sub}/p$ requirement for electrons in the endcap region, because these are most sensitive to the isolation of the electron. In order to reduce the dependence on the Monte Carlo modelling of electromagnetic showers in the lead-glass calorimeter, the source dependence of the efficiency due to these selection criteria was estimated

by combining the energy deposited by isolated electrons in low multiplicity events in the data with the energy deposited by nearby particles in the regions around prompt muons in simulated hadronic Z^0 decays. The energy deposited by the muon itself was subtracted. The distribution of the energy deposited around a muon for muons from a given source is expected to be the same as for electrons coming from this source with the same p and p_t. The energy around muons in simulated events was in reasonable agreement with the observed energy around muons in hadronic Z^0 decays in the data. The surrounding energy in simulated events was scaled by a factor $\mathcal{F}$, to improve agreement with the data. The fitted value of $\mathcal{F}$ was 0.9 ± 0.2 in the barrel region, and 0.9 ± 0.3 in the endcap. The error in the source dependence includes Monte Carlo statistics and the effect of varying $\mathcal{F}$ by one standard deviation. The source dependence of the identification efficiency due to the barrel $E_{\rm cone}/p$ and endcap $|\theta_{\rm track} - \theta_{\rm cluster}|$ requirements were estimated in a similar manner.

Simulated events were used to predict the small additional contributions to the source dependence due to demanding that the track be associated with a cluster in the calorimeter, and the presampler requirement. A systematic error was assigned based on the agreement between Monte Carlo events and data for these variables. The Monte Carlo prediction for the $N_{\rm samp}$ requirement was also taken, in this case with the full source dependence assumed as a systematic error. An additional systematic error based on the difference in the efficiency of a $\mathrm{d}E/\mathrm{d}x$ requirement for isolated electrons in low multiplicity events and for minimum ionizing pions was included.

The resulting ratios between the average electron identification efficiencies for different sources were consistent for electrons in the barrel and endcap regions. For tracks with $p > 2$ GeV/c and $p_t > 0.8$ GeV/c they were found to be: $\epsilon(\mathrm{b} \to \mathrm{c} \to \mathrm{e})/\epsilon(\mathrm{b} \to \mathrm{e}) = 0.87 \pm 0.04$ and $\epsilon(\mathrm{c} \to \mathrm{e})/\epsilon(\mathrm{b} \to \mathrm{e}) = 0.80 \pm 0.07$. The results for lower p_t were within 2% of these values. The identification efficiencies $\epsilon(\mathrm{b} \to \tau^- \to \mathrm{e}^-)$ and $\epsilon(\mathrm{b} \to \mathrm{J}/\psi \to \mathrm{e})$ were assumed equal to $\epsilon(\mathrm{b} \to \mathrm{e})$ as predicted by Monte Carlo simulation.

3 Modelling of heavy flavour semileptonic decay

The analysis relies on understanding the relative rates and the p and p_t distributions for the various sources of prompt leptons. Particular attention was therefore paid to the modelling of heavy flavour fragmentation and semileptonic decays, using the procedures described in detail in [13]. The semileptonic decay model is important not only in Z^0 decays, where it has some influence on the p spectrum and strongly affects the p_t distribution, it is equally relevant for lower centre-of-mass energy experiments where the measurements of the semileptonic branching ratios have been made. In both cases, the observed lepton momentum spectrum includes contributions from $\mathrm{b} \to \ell^-$ and $\mathrm{b} \to \mathrm{c} \to \ell$ decays. The measured branching ratios, $Br(\mathrm{b} \to \ell^-)$ and $Br(\mathrm{b} \to \mathrm{c} \to \ell)$, therefore depend on the theoretical models used to predict the momentum distribution for these two components in a correlated way. Taking into account this correlation can lead to a reduction of the systematic error in the measurement of $\Gamma_{\mathrm{b\bar{b}}}/\Gamma_{\rm had}$ from Z^0 decays [14, 13]. However, since the dominant cascade component, $\mathrm{b} \to \mathrm{c} \to \ell^+$, contributes to the asymmetry with the opposite sign to the direct $\mathrm{b} \to \ell^-$ component, a proper account of this correlation leads to an increased estimated systematic error in this analysis.

Measurements of b hadron semileptonic branching ratios by the CLEO Collaboration using $\Upsilon(4S)$ decays were taken [15]. Full details of the theoretical models have been provided. The central values of the asymmetry measurements in this publication assume the branching ratios measured by CLEO using the model of Altarelli *et al.*, ACCMM [16]. Branching ratio measurements using the model of Isgur *et al.* [17], ISGW, and a momentum spectrum derived from this model with the fraction of D^{**} decays fitted by CLEO to be 32%, denoted ISGW**, are used to assess the systematic error.

The error on the value of $Br(\mathrm{b} \to \ell^-)$ was inflated to take into account the possible difference in average semileptonic branching ratio for the composition of b hadrons produced in $\Upsilon(4S)$ and Z^0 decays [13]. The values used are given in table 1. The CLEO branching ratio $Br(\mathrm{b} \to \mathrm{c} \to \ell)$ is measured for the sum of all cascade processes, while for the asymmetry analysis the two branching

ratios $Br(\mathrm{b} \to \mathrm{c} \to \ell^+)$ and $Br(\mathrm{b} \to \overline{\mathrm{c}} \to \ell^-)$ must be estimated. The factors by which the CLEO result was multiplied to give these two branching ratios in Z^0 decays are given in table 1. These factors take into account the different semileptonic branching ratios of the c hadrons expected in $\mathrm{B_d}$, B^+, $\mathrm{B_s}$ and Λ_b decays, and the fraction of b quark decays in which a $\overline{\mathrm{c}}$ antiquark is produced in addition to a c quark ($15 \pm 5\%$) [13, 18]. The values of $Br(\mathrm{b} \to \tau^- \to \ell^-)$ and $Br(\mathrm{b} \to \mathrm{J}/\psi \to \ell)$ [13] are also given in table 1. The values are based on phase space considerations [18] and world average branching ratios [19].

In treating $\mathrm{c} \to \ell^+$ decays, the ACCMM and ISGW models were again used for the central value of the asymmetry and in assessing the systematic error respectively. However, no correlated measurements of the semileptonic branching ratio were available in this case. The ACCMM model parameters used were from a fit to semileptonic D decay measurements from the DELCO Collaboration [20]. Both models are in reasonable agreement with these data, and the differences between them give an estimate of the range of spectra the data can support. The branching ratio $Br(\mathrm{c} \to \ell^+)$ was derived from world average values of measured c hadron semileptonic branching ratios and lifetimes [19] and the fractions of c hadron species produced in $\mathrm{c\overline{c}}$ events predicted by the JETSET Monte Carlo program. The value used is given in table 1.

The $\mathrm{b\overline{b}}$ and $\mathrm{c\overline{c}}$ JETSET Monte Carlo events were reweighted according to the lepton momentum in the hadron rest frame to reproduce the distributions predicted by the semileptonic decay models.

	ISGW	ACCMM	ISGW**
$Br(\mathrm{b} \to \ell^-)$ (%)	10.1	10.5 ± 0.5	11.1
$Br(\mathrm{b} \to \mathrm{c} \to \ell)$ from CLEO (%)	11.1	9.7 ± 1.0	9.3
$Br(\mathrm{b} \to \mathrm{c} \to \ell^+)(\mathrm{Z}^0)/Br(\mathrm{b} \to \mathrm{c} \to \ell)(\Upsilon(4S))$	0.81 ± 0.09		
$Br(\mathrm{b} \to \overline{\mathrm{c}} \to \ell^-)(\mathrm{Z}^0)/Br(\mathrm{b} \to \mathrm{c} \to \ell)(\Upsilon(4S))$	0.11 ± 0.04		
$Br(\mathrm{c} \to \ell^+)$ (%)	9.6 ± 1.1		
$Br(\mathrm{b} \to \tau^- \to \ell^-)$ (%)	0.5 ± 0.2		
$Br(\mathrm{b} \to \mathrm{J}/\psi \to \ell)$ (%)	0.14 ± 0.04		

Table 1: Branching ratio values, including the factors used to convert the value of $Br(\mathrm{b} \to \mathrm{c} \to \ell)$ measured by CLEO into values of $Br(\mathrm{b} \to \mathrm{c} \to \ell^+)$ and $Br(\mathrm{b} \to \overline{\mathrm{c}} \to \ell^-)$ in Z^0 decays. The derivation of these values is discussed in the text.

4 Measurements of A_{FB}^{b} and A_{FB}^{c}

All the measurements presented here use the experimental variable $y = -Q\cos\theta_{\mathrm{thrust}}$. The differential cross-section has the form:

$$\frac{\mathrm{d}\sigma}{\mathrm{d}y} \propto \sum_s f_s \left(1 + y^2 + \frac{8}{3} A_{FB}^s \; y\right) \epsilon_s(y). \tag{3}$$

Here the sum runs over all sources of lepton candidates, f_s is the fraction of lepton candidates from a given source, A_{FB}^s is the asymmetry of this source, and ϵ_s is the acceptance for this source as a function of y. The acceptance functions, $\epsilon_s(y)$, are normalised to unity and the average identification efficiencies are absorbed into the fractions f_s. For non-prompt backgrounds, the acceptance function, $\epsilon_s(y)$, also takes into account variations in the background rate, for example due to the distribution of material in the detector. Although the detector is not precisely symmetric as a function of $\cos\theta$, its response is expected to be the same for positive and negative particles to a very good approximation, and so the functions ϵ_s are taken to be even functions of y. The assumption that the functions ϵ_s have the same y dependence for all sources of prompt leptons is supported by Monte Carlo studies. Assuming

that non-prompt leptons also have the same acceptance function, equation (3) can be written:

$$\frac{\mathrm{d}\sigma}{\mathrm{d}y} = C\left(1 + y^2 + \frac{8}{3}A_{FB}^{\mathrm{obs}}\, y\right)\epsilon(|y|). \tag{4}$$

In this expression, the normalizing constant, C, is independent of the asymmetry of the sample, A_{FB}^{obs}, because the acceptance function for all sources, $\epsilon(y)$, is an even function of y. The asymmetry of the sample, $A_{FB}^{\mathrm{obs}} = \sum_s f_s A_{FB}^s$, is given by:

$$A_{FB}^{\mathrm{obs}} = (f_{\mathrm{b}\to\ell^-} + f_{\mathrm{b}\to\tau^-\to\ell^-} - f_{\mathrm{b}\to\mathrm{c}\to\ell^+} + f_{\mathrm{b}\to\overline{\mathrm{c}}\to\ell^-})A_{FB}^{\mathrm{b,mix}} - f_{\mathrm{c}\to\ell^+}A_{FB}^{\mathrm{c}} + f_{\mathrm{back}}A_{FB}^{\mathrm{back}}. \tag{5}$$

If the non-prompt background does not follow the distribution $(1 + y^2 + (8/3)A_{FB}^{\mathrm{back}}y)\epsilon(|y|)$, then equations (4) and (5) still hold if the background is first subtracted from the distribution, so that $f_{\mathrm{back}} = 0$.

In each of the measurements presented below, equation (5) was used to relate the observed asymmetry of the sample to the underlying quark asymmetries. The fractions, f_s, of each prompt source were calculated using the semileptonic branching ratios given in table 1, and kinematic and geometrical efficiencies derived from the JETSET Monte Carlo samples with Peterson fragmentation, reweighted to take account of the theoretical models of semileptonic decay described in section 3. For electrons, the differences in electron identification efficiency for different sources were also included in the calculation of the fractions. The contribution from non-prompt leptons is discussed for each measurement. As is described below, fits can be constructed such that the form of $\epsilon(|y|)$ does not need to be known. However, correcting for the acceptance as a function of y allows a check that the assumed form of the cross section is valid.

Except where it was left free, the charm asymmetry was taken to have its Standard Model value for the appropriate centre-of-mass energy, as predicted by the program ZFITTER [21], with $M_{\mathrm{Z}} = 91.187\,\mathrm{GeV}/c^2$, a top quark mass of $132\,\mathrm{GeV}/c^2$, a Higgs boson mass of $300\,\mathrm{GeV}/c^2$ and $\alpha_s = 0.12$ [22]. For $\sqrt{s} = 91.24\,\mathrm{GeV}$, these parameters lead to a value of $A_{FB}^{\mathrm{c}} = 0.056$. The predictions of ZFITTER were also used for the fraction of hadronic Z^0 decays to $\mathrm{b\overline{b}}$ and $\mathrm{c\overline{c}}$: $\Gamma_{\mathrm{b\overline{b}}}/\Gamma_{\mathrm{had}} = 0.217$ and $\Gamma_{\mathrm{c\overline{c}}}/\Gamma_{\mathrm{had}} = 0.171$. The dependence of the measurements on the values of A_{FB}^{c}, $\Gamma_{\mathrm{b\overline{b}}}$ and $\Gamma_{\mathrm{c\overline{c}}}$ was also considered.

Events with more than one lepton candidate were considered once per candidate. It was verified that this made a negligible difference to the statistical error compared to allowing only one candidate per event.

4.1 Measurements using high p_t muons

A sample of 6614 identified muon candidates with $p > 3\,\mathrm{GeV}/c$ and $p_t > 1.0\,\mathrm{GeV}/c$ was selected from the on-peak data. This kinematic region is expected to be dominated by $\mathrm{b}\to\ell^-$ decays.

The hadronic background in 12 bins of equal width in y was estimated using the fake probability per track multiplied by the total number of tracks in this kinematic region as described in section 2.4. The distribution of y for all muon candidates is shown in figure 4, with the expected background superimposed. As can be seen from this figure, the approximation that the background and prompt muons both follow the form of equation (4) is invalid. This is because the fake probability per track depends strongly on the distribution of material in the detector. The predicted background in bins of y was therefore subtracted from the sample of muon candidates before fitting for A_{FB}^{obs}.

The background subtracted distribution was corrected bin-by-bin in y for the muon identification efficiency to obtain the expected y distribution for prompt muons. The efficiency was also assumed to be a symmetric function of y. The corrected distribution of y for prompt muons is shown in figure 5.

The asymmetry of this corrected distribution was obtained using a binned χ^2 fit to the form $1 + y^2 + (8/3)A_{FB}^{\mathrm{obs}}\, y$ normalised to the integral of the corrected distribution. The fit took into account the correlated errors for bins with the same value of $|y|$ arising from the assumed symmetry of the fake probability per track and efficiency. The only free parameter was the effective asymmetry, whose fitted

value was $A_{FB}^{\rm obs} = 0.056 \pm 0.014\,({\rm stat})$, corresponding to the curve shown in figure 5. The χ^2/d.o.f. is 14.9/11, indicating that the data are consistent with the predicted differential cross section. The calculated fractions of each source in the sample are given in table 2. From equation (5) with $f_{\rm back} = 0$, and the fractions of other sources rescaled to sum to unity, the b asymmetry was found to be:

$$A_{FB}^{\rm b,mix} = 0.076 \pm 0.018\,({\rm stat}).$$

This measurement was also made using the two off-peak data samples. The average value of $\sqrt{s}$ for events containing high p and p_t muon candidates was calculated for each sample. The results are given in table 3.

Muons			
	$p_t > 1$ GeV/c	$p_t < 1$, $p > 6$ GeV/c	$p_t < 1$, $p < 6$ GeV/c
Number of events	6614	7948	10363
$f_{\rm back}$	0.121	0.345	0.593
$f_{\rm b\to\ell^-}$	0.727	0.250	0.089
$f_{\rm b\to\tau^-\to\ell^-}$	0.009	0.012	0.009
$f_{\rm b\to c\to\ell^+}$	0.071	0.113	0.151
$f_{\rm b\to\bar{c}\to\ell^-}$	0.008	0.014	0.021
$f_{\rm b\to J/\psi\to\ell}$	0.016	0.002	0.000
$f_{\rm c\to\ell^+}$	0.048	0.263	0.136
Electrons			
	$p_t > 0.8$ GeV/c	$p_t < 0.8$, $p > 6$ GeV/c	$p_t < 0.8$, $p < 6$ GeV/c
Number of events	4792	2079	4539
$f_{\rm conv}$	0.024	0.039	0.249
$f_{\rm misID}$	0.036	0.180	0.054
$f_{\rm b\to\ell^-}$	0.745	0.327	0.137
$f_{\rm b\to\tau^-\to\ell^-}$	0.013	0.015	0.018
$f_{\rm b\to c\to\ell^+}$	0.093	0.116	0.264
$f_{\rm b\to\bar{c}\to\ell^-}$	0.011	0.012	0.035
$f_{\rm b\to J/\psi\to\ell}$	0.012	0.002	0.001
$f_{\rm c\to\ell^+}$	0.067	0.307	0.243

Table 2: The fractions of muon and electron candidates coming from different sources for representative p–p_t regions.

4.2 Measurement using high p_t electrons

A second sample of events from the on-peak data, enriched in $\mathrm{b} \to \ell^-$ decays, consisted of 4792 identified electron candidates with $p > 2$ GeV/c and $p_t > 0.8$ GeV/c. The distribution of the electron candidates as a function of y is shown in figure 6. In contrast to the muons, the electron identification efficiency varies significantly with y. This is dominated by the geometrical acceptance for electron candidates. However the assumption that the acceptance for background follows the same form $\epsilon(|y|)$ as prompt electrons was tested by fits to the data in different regions of y and was found to be valid. In view of these two features, the asymmetry was measured using an unbinned maximum likelihood fit. From equation (4), $A_{FB}^{\rm obs}$ can be obtained by maximising the log likelihood:

$$\ln \mathcal{L} = \sum_j \ln[C\epsilon(|y_j|)] + \sum_j \ln[1 + y_j^2 + \frac{8}{3} A_{FB}^{\rm obs} y_j], \qquad (6)$$

	$\langle\sqrt{s}\rangle$(GeV)	A_{FB}^{c} (predicted)	$A_{FB}^{\mathrm{b,mix}}$
Muons	89.65	-0.030	0.064 ± 0.054
	91.24	0.056	0.076 ± 0.018
	92.75	0.111	0.173 ± 0.045
Electrons	89.67	-0.029	0.039 ± 0.063
	91.24	0.056	0.072 ± 0.023
	92.75	0.111	-0.012 ± 0.057
Combined	89.66	-0.029	0.054 ± 0.041
	91.24	0.056	0.075 ± 0.014
	92.75	0.111	0.100 ± 0.036

Table 3: Results from one parameter fits to high p_t lepton data for $A_{FB}^{\mathrm{b,mix}}$. The Standard Model values of $\Gamma_{\mathrm{b\overline{b}}}/\Gamma_{\mathrm{c\overline{c}}}$ and A_{FB}^{c} are assumed. The errors are statistical only.

where the sum is over all electron candidates, j, in the sample and A_{FB}^{obs} is the only free parameter in the fit. The first term is a constant for a given set of events, so that the efficiency as a function of y does not need to be known, and the background follows the same form as the prompt leptons and so does not need to be subtracted before fitting for the effective asymmetry of the sample. The fit result was $A_{FB}^{\mathrm{obs}} = 0.045 \pm 0.015\,(\mathrm{stat})$. The fractions of events coming from the various sources are given in table 2. Electrons from Dalitz decays are included with the conversions and denoted "conv". Hadrons misidentified as electrons are denoted "misID". The Dalitz decays, conversions and misidentified hadrons were assumed to have zero asymmetry. From equation (5), the forward-backward asymmetry of $\mathrm{e^+e^-} \to \mathrm{b\overline{b}}$ was found to be:

$$A_{FB}^{\mathrm{b,mix}} = 0.072 \pm 0.023\,(\mathrm{stat}).$$

Deviations from the assumption that the conversion and misidentified hadron backgrounds have the same acceptance function and zero asymmetry were taken into account in evaluating the systematic errors, as discussed in section 5.

The asymmetry was also measured using a binned χ^2 fit to this sample, following the method used for muon candidates in the previous section. Backgrounds from hadrons misidentified as electrons and electrons from untagged photon conversions were estimated from the data and subtracted bin-by-bin in y from the observed angular distribution. The background from Dalitz decays and other electrons that do not come from decays of b or c hadrons were estimated from simulated events and were also subtracted. The resulting distribution was then corrected for the angular variation of the efficiency. The angular variation of the kinematic and geometrical efficiency was calculated using the Monte Carlo simulation of b and c events. The electron identification efficiencies were determined from the data, separately for electrons in the barrel and endcap parts of the calorimeter, and combined in bins of $|y|$. The efficiency corrected distribution is shown in figure 7. The result of a binned χ^2 fit to this corrected y distribution is $A_{FB}^{\mathrm{obs}} = 0.047 \pm 0.016\,(\mathrm{stat})$, with a $\chi^2/\mathrm{d.o.f.} = 3.6/9$, again indicating that the predicted form of the differential distribution describes the data. From equation (5) with $f_{\mathrm{back}} = 0$, this value of A_{FB}^{obs} gives a consistent result for the $\mathrm{b\overline{b}}$ asymmetry of $A_{FB}^{\mathrm{b,mix}} = 0.071 \pm 0.023\,(\mathrm{stat})$.

The unbinned maximum likelihood fit was also performed using the two off-peak data samples. The results are given in table 3.

4.3 Combination of results using high p_t muons and electrons

The results of the binned χ^2 fit to the corrected y distribution for muon candidates and the unbinned maximum likelihood fit to the electron candidates for $\langle\sqrt{s}\rangle = 91.24$ GeV were combined to give:

$$A_{FB}^{\mathrm{b,mix}} = 0.075 \pm 0.014\,(\mathrm{stat}).$$

The combined results for the off-peak data are given in table 3.

4.4 Measurement from a fit in p, p_t and $\cos\theta_{\mathrm{thrust}}$ for muons and electrons

Relaxing the p_t cuts imposed for the measurements described above yields samples of 24485 muon candidates with $p > 3$ GeV/c, and 11410 electron candidates with $p > 2$ GeV/c, from the on-peak data. The extra misassociation cut for muons described in section 2.4 was applied in this case. This reduces the number of muons with $p_t > 1.0\,\mathrm{GeV}/c$ from 6614 to 6574. Taking advantage of the different relative contributions from $\mathrm{b} \to \ell^-$, cascade, $\mathrm{c} \to \ell^+$ and non-prompt backgrounds as a function of p and p_t it is possible to measure the asymmetry of $\mathrm{b\overline{b}}$ and $\mathrm{c\overline{c}}$ events simultaneously. For illustration, the fractions of leptons from different sources in the low p_t region with high or low p are given in table 2. The shapes of the p–p_t distributions can be seen in figure 8.

A χ^2 function which compares the expected and observed asymmetry in bins of p, p_t and $|y|$ was constructed as follows:

$$\chi^2(p, p_t, |y|) = \sum_i \frac{1}{\sigma_i^2} \left[\frac{N_i^F - N_i^B}{N_i^F + N_i^B} - \frac{8}{3} A_{FB\,i}^{\mathrm{obs}} \frac{|y_i|}{1 + y_i^2} \right]^2 . \qquad (7)$$

Here N_i^F (N_i^B) are the numbers of forward (backward) events in bin i, after subtracting the predicted non-prompt backgrounds. $A_{FB\,i}^{\mathrm{obs}}$ is given by equation (5), with $f_{\mathrm{back}} = 0$. The sum is over 6 equal bins of $|y|$ between 0 and 0.9 and over coarse bins of p and p_t for electrons and muons separately [4]. The p and p_t bins are different for the two lepton species. They were chosen to give roughly equal numbers of events in each bin. This approach has the advantage that the exact form of the efficiency is not needed, so long as the efficiency does not vary greatly across the bin in y. The value of y_i for the bin was taken to be the centre of the bin. The only free parameters in the fit were $A_{FB}^{\mathrm{b,mix}}$ and A_{FB}^{c}.

The principle is illustrated in figure 9, in which the ratio $(N^F - N^B)/(N^F + N^B)$, in bins of $|y|$ for the high p_t lepton samples, is compared to the fitted function $8A_{FB}^{\mathrm{obs}}|y|/3(1+y^2)$, where A_{FB}^{obs} is the only free parameter.

The fractions of prompt leptons from different sources were taken to be functions of p and p_t only, and not of $\cos\theta_{\mathrm{thrust}}$. The forward and backward muon background in each bin was predicted from the fake probability per track estimated in the bin of p, p_t and $|y|$, multiplied by the total number of forward and backward tracks in that bin. As described in section 2.4, although the fake probability per track was assumed to be a symmetric function of y, the predicted background has the same asymmetry as all tracks in the data. The fractions of electron candidates which were misidentified hadrons were estimated by fits to the data in each bin of p and p_t. The fraction was allowed to be different for electron candidates in the barrel and endcap regions of the detector, but was otherwise assumed to be independent of y. The conversion tagging efficiency, and the rate of incorrectly tagging a prompt electron as a converted photon were found from Monte Carlo simulation as a function of p and p_t. They were used to predict the numbers of untagged conversions in the sample from the numbers of tagged conversions in each bin of p, p_t and y. The untagged conversions were assumed to have zero asymmetry.

The term σ_i includes all errors of a statistical nature. This is dominated by the statistical error from the lepton candidates in the data, but includes small contributions from Monte Carlo statistics in deriving the fractions of each prompt source in each bin of p and p_t, and contributions from both data and Monte Carlo in estimating the various non-prompt backgrounds.

[4] A term (bin width)$^2/12$ in the denominator of the predicted asymmetry has been neglected.

	$A_{FB}^{\mathrm{b,mix}}$	A_{FB}^{c}	Correlation coefficient	χ^2/d.o.f.
Muons only	0.081 ± 0.017	0.055 ± 0.037	0.30	147/148
Electrons only	0.052 ± 0.022	-0.060 ± 0.050	0.28	67/70
Combined	0.070 ± 0.014	0.014 ± 0.030	0.29	218/220

Table 4: Results of two parameter fits for $A_{FB}^{\mathrm{b,mix}}$ and A_{FB}^{c}. The errors are statistical only. Only the on-peak data were used, with $\langle\sqrt{s}\rangle = 91.24$ GeV.

The results of the two parameter fit using electron data, muon data and the combined data set, together with the correlation coefficient between the parameters and the χ^2/d.o.f. values, are given in table 4. The errors in the table are statistical only. The results using muons and electrons are consistent at the 1.9 standard deviation level for A_{FB}^{c}, and 1.1 standard deviations for $A_{FB}^{\mathrm{b,mix}}$. There is no indication that this difference has anything other than a statistical origin. This is supported by the values of χ^2/d.o.f. for the three fits. The numbers of events in the off-peak data samples were insufficient to perform a two parameter fit.

Consistency checks with the one parameter fit results presented above were made by fixing A_{FB}^{c} to its Standard Model value, while restricting the fit to one p–p_t bin corresponding to the b-enriched region used for the one parameter fits. The additional cut to reject misassociation background in the muon sample was relaxed for this comparison. The results were $A_{FB}^{\mathrm{b,mix}} = 0.075 \pm 0.018$ for muons with $p > 3$ GeV/c and $p_t > 1.0$ GeV/c and $A_{FB}^{\mathrm{b,mix}} = 0.070 \pm 0.023$ for electrons with $p > 2$ GeV/c and $p_t > 0.8$ GeV/c, in good agreement with the values given above. As a further check, the fit over the full p_t range in bins of p and p_t was performed with A_{FB}^{c} fixed to its Standard Model value, resulting in a value of $A_{FB}^{\mathrm{b,mix}} = 0.075 \pm 0.013$, for muons and electrons combined, again in good agreement with the result using high p_t leptons.

5 Systematic uncertainties

The dominant systematic errors arise from uncertainties in the modelling of b and c hadron production and decay, and from electron and muon identification and backgrounds. The studies of possible systematic effects are described in the following sections, and the resulting systematic errors are listed in table 5. The common systematic errors were taken into account when combining the results of the one parameter fits to high p_t muons and electrons. The systematic errors quoted for the two parameter fit are in each case for the result of a simultaneous fit to muon and electron data.

5.1 Modelling of the production and decay of b and c hadrons

Decay models and branching ratios were discussed in section 3. The decay models and values of the b hadron semileptonic branching ratios were varied simultaneously. For example, when reweighting the Monte Carlo events to reproduce the momentum spectrum of the ISGW model, the CLEO measured branching ratios for the ISGW model were used. The resulting error is denoted "b decay model" in the table.

The central values of the branching ratios $Br(\mathrm{b} \to \ell^-)$, $Br(\mathrm{b} \to \mathrm{c} \to \ell^+)$ and $Br(\mathrm{b} \to \overline{\mathrm{c}} \to \ell^-)$, measured using the ACCMM model, were in addition varied by the errors given in table 1. These include CLEO statistical errors, CLEO systematic errors not related to modelling, and the extra errors introduced by using these results in Z^0 decays, including variation of the fraction of $\mathrm{b} \to \overline{\mathrm{c}}$ decays, and the variations of $\mathrm{B_s}$ and Λ_b properties.

	Fit for $A_{FB}^{\mathrm{b,mix}}$ using		Two parameter fit for	
	μ events	e events	$A_{FB}^{\mathrm{b,mix}}$	A_{FB}^{c}
b decay model	0.0021	0.0019	0.0022	0.0062
c decay model	0.0009	0.0009	0.0007	0.0004
$Br(\mathrm{b} \to \ell^-)$	0.0011	0.0013	0.0008	0.0019
$Br(\mathrm{b} \to \mathrm{c} \to \ell^+)$ and $Br(\mathrm{b} \to \overline{\mathrm{c}} \to \ell^-)$	0.0021	0.0025	0.0014	0.0060
$Br(\mathrm{c} \to \ell^+)$	0.0009	0.0012	0.0009	0.0013
$Br(\mathrm{b} \to \tau^- \to \ell^-)$	0.0001	0.0002	0.0000	0.0014
$Br(\mathrm{b} \to \mathrm{J}/\psi \to \ell)$	0.0004	0.0002	0.0003	0.0001
ϵ_{b}	0.0002	0.0005	0.0002	0.0013
ϵ_{c}	0.0002	0.0005	0.0003	0.0016
b and c modelling	0.0034	0.0038	0.0030	0.0093
Total muon background rate	0.0012	–	0.0012	0.0122
Muon background shape	–	–	0.0009	0.0060
Muon acceptance	0.0014	–	–	–
Muon identification	0.0018	–	0.0015	0.0137
Electron source dependence	–	0.0017	0.0003	0.0016
Conversions and Dalitz decays	–	0.0004	0.0017	0.0072
Hadron misidentified as e	–	0.0004	0.0005	0.0049
Electron identification	–	0.0018	0.0018	0.0089
Modelling of detector resolution	0.0011	0.0010	0.0004	0.0010
Track charge error	0.0016	0.0021	0.0012	0.0026
Quark direction resolution	0.0010	0.0010	0.0010	0.0010
Detector effects	0.0022	0.0025	0.0016	0.0030
Total error within Standard Model	0.0045	0.0048	0.0041	0.0190
$A_{FB}^{\mathrm{c}}, \Gamma_{\mathrm{c\overline{c}}}, \Gamma_{\mathrm{b\overline{b}}}$	see text		0.0034	0.0060

Table 5: Systematic errors. The first two columns give the errors for one parameter fits for $A_{FB}^{\mathrm{b,mix}}$ to high p_t muon and electron samples. The second two columns give the errors for the two parameter fit for $A_{FB}^{\mathrm{b,mix}}$ and A_{FB}^{c} using muon and electron data together. Subtotals for each category and the total error within the framework of the Standard Model are quoted. The last line indicates the error arising from experimental uncertainties in parameters taken from the Standard Model prediction.

The $\mathrm{c} \to \ell^+$ decay model and branching ratio were varied independently, since no correlated measurements using the ACCMM and ISGW models are available. The ACCMM and ISGW models give a reasonable indication of the variation in the lepton momentum spectrum tolerated by the DELCO data [20]. Other branching ratios were also varied by the errors given in table 1.

The error due to fragmentation was estimated by varying ϵ_{b} in the range 0.0025 to 0.0095, and ϵ_{c} in the range 0.030 to 0.070. This corresponds to $\langle x_E \rangle_{\mathrm{b}} = 0.70 \pm 0.02$ and $\langle x_E \rangle_{\mathrm{c}} = 0.51 \pm 0.02$ [8].

5.2 Uncertainties arising from muon identification and background

The total hadronic background in the muon sample was varied by $\pm 13\%$. The different sources of backgrounds have different distributions in p and p_t. For the simultaneous measurement of $A_{FB}^{\mathrm{b,mix}}$ and A_{FB}^{c}, uncertainties in the shape of the p, p_t distribution of background muons were therefore estimated by varying the rates of misassociation and punchthrough backgrounds by their uncertainties, $\pm 25\%$ and $\pm 50\%$ respectively.

For the one parameter fit, where the data were explicitly corrected for the identification efficiency

as a function of $\cos\theta$, uncertainties in the modelling of the identification efficiency were taken into account by comparing muon pair events in data and Monte Carlo simulation. Uncertainties in the overall efficiency and bin-to-bin differences were considered. The uncertainty due to Monte Carlo statistics in calculating the acceptance and kinematic efficiency in order to derive the fractions of candidates from different sources is also included as a systematic error for this measurement. These efficiency and acceptance uncertainties are combined and denoted "Muon acceptance" in the table.

5.3 Uncertainties arising from electron identification and background

The fractions of events from different sources of prompt electrons were reevaluated using the estimated variations in relative identification efficiencies described in section 2.5. This error is quoted as electron source dependence.

The systematic uncertainties of 5% in the conversion tagging efficiency and 10% in the purity of the tagged conversion sample were taken into account. The uncertainty in the rate of electrons from Dalitz decays was included in the error due to the rate of untagged conversions. The untagged conversions were assumed to be symmetric in y. This assumption was tested using the tagged conversions. For example, for the high p_t sample, the tracks tagged as conversions had an observed asymmetry of 0.017 ± 0.048(stat), consistent with zero.

In calculating $A_{FB}^{\mathrm{b,mix}}$ using the one parameter likelihood fit, the photon conversions in the sample were assumed to be produced with the angular distribution $(1+y^2)$. However, the distribution of material in the detector means that the probability that a photon will convert in the detector is not constant as a function of $\cos\theta$. The possible systematic bias was estimated by refitting the electron sample using the measured angular distribution of photon conversions. The resulting difference in the observed asymmetry was negligible.

The percentage of misidentified hadrons, 3.6%, in the electron sample was varied by $\pm 0.3\%$ for the high p_t measurement. For the two parameter fit, the error on the fraction of misidentified hadrons varied from bin to bin in p and p_t, and the errors were expected to be almost entirely uncorrelated. They were therefore included in the fit bin by bin. This makes a negligible difference to the statistical error from the fit. In the one parameter likelihood fit, it was assumed that the acceptances for the various sources of electrons followed the same function of y. However, the fraction of misidentification background present in the sample decreases with $|y|$. To determine the sensitivity of the measurement to this variation, the background fraction was calculated in three bins of $|y|$, and used to correct the asymmetry in each bin. A weighted average of the asymmetry measured in the three bins was calculated. The difference from the value found assuming a constant background fraction was found to be 0.0003. This was included in the systematic error.

The misidentified hadron background was assumed to be symmetric. An uncertainty due to a possible 4% asymmetry in the background was included in the systematic error [23]. An estimate of the possible asymmetry of the misidentified hadron background was made using a sample of events with tracks having a value of E/p characteristic of background but satisfying all the other electron identification and kinematic requirements. The number of forward and backward tracks in the high p_t region had an asymmetry of -0.014 ± 0.034 (stat).

5.4 Detector resolution effects not connected with lepton identification

Inadequacies of the modelling of the detector resolution in the Monte Carlo simulation for the measurement of p and p_t were estimated by scaling the deviation of track parameters from their true values by a factor of 1.4. This factor has been found to give better agreement between data and simulation for distributions of resolution dependent quantities, but the changes in the kinematic efficiencies resulted in only a small difference in the result, which was assigned as a systematic error.

The effect of the resolution of the thrust axis direction was estimated using the JETSET Monte Carlo program. The probability of wrongly assigning the charge of a track was estimated to be less

than 0.2%. This value was used to estimate a systematic uncertainty due to the incorrect signing of the thrust axis direction.

5.5 Additional uncertainties for measurements using the off-peak data samples

The kinematic efficiencies used in the analysis were evaluated using Monte Carlo samples generated with $\sqrt{s} \approx M_{\rm Z}$. As the off-peak data were accumulated over a range of values of $\sqrt{s}$ within about ± 3 GeV of $M_{\rm Z}$, a small additional systematic error was assigned to cover possible relative variations in the kinematic efficiencies of the different sources. Other systematic errors were evaluated using the procedures described above. The total systematic errors are quoted in table 6.

5.6 Dependence on Standard Model assumptions

The results of the one parameter fits for $A_{FB}^{\rm b,mix}$ depend on $\Gamma_{\rm b\overline{b}}$, $\Gamma_{\rm c\overline{c}}$ and $A_{FB}^{\rm c}$. Writing $\lambda = \Gamma_{\rm c\overline{c}}/\Gamma_{\rm b\overline{b}}$, the dependence of the combined muon and electron results is:

$$\begin{aligned} A_{FB}^{\rm b,mix}(\langle\sqrt{s}\rangle = 89.66) &= 0.0526 + 0.0043\lambda + 0.106\lambda A_{FB}^{\rm c}, \\ A_{FB}^{\rm b,mix}(\langle\sqrt{s}\rangle = 91.24) &= 0.0658 + 0.0055\lambda + 0.105\lambda A_{FB}^{\rm c}, \\ A_{FB}^{\rm b,mix}(\langle\sqrt{s}\rangle = 92.75) &= 0.0857 + 0.0061\lambda + 0.105\lambda A_{FB}^{\rm c}. \end{aligned}$$

The central results assume the value of $\lambda = 0.171/0.217$, and values of $A_{FB}^{\rm c}(\langle\sqrt{s}\rangle = 89.66) = -0.029$, $A_{FB}^{\rm c}(\langle\sqrt{s}\rangle = 91.24) = 0.056$ and $A_{FB}^{\rm c}(\langle\sqrt{s}\rangle = 92.75) = 0.111$.

The model dependence is reduced by the two parameter fit for $A_{FB}^{\rm b,mix}$ and $A_{FB}^{\rm c}$. In this case the statistical error for $A_{FB}^{\rm b,mix}$ includes uncertainty in the value of $A_{FB}^{\rm c}$. The dependence of the results of this fit on λ was determined to be:

$$\begin{aligned} A_{FB}^{\rm b,mix} &= 0.0552 + 0.0187\lambda, \\ A_{FB}^{\rm c} &= 0.0628 - 0.0958\lambda + 0.0437\lambda^2. \end{aligned}$$

The central values again assume the value of $\lambda = 0.171/0.217$. A systematic error was assigned assuming a variation of $\Gamma_{\rm c\overline{c}}/\Gamma_{\rm b\overline{b}}$ of 22%, which is due almost entirely to the uncertainty in $\Gamma_{\rm c\overline{c}}$ [9,13].

6 Results and conclusions

The true $\rm b\overline{b}$ forward-backward asymmetry, $A_{FB}^{\rm b}$, is given by $A_{FB}^{\rm b} = A_{FB}^{\rm b,mix}/(1-2\chi)$, where χ is the average $\rm B^0\overline{B^0}$ mixing parameter in $\rm Z^0$ decays. The measured values of $A_{FB}^{\rm b,mix}$ were corrected using a value of $\chi = 0.119 \pm 0.012$ [24]. This is the average mixing parameter measured using hadronic $\rm Z^0$ decays including two lepton candidates at LEP, and is therefore measured from event samples with the same composition of decaying b hadrons as this analysis.

The results of the one parameter fits for $A_{FB}^{\rm b,mix}$ to the high p_t muon and electron samples assuming the Standard Model predictions for $\Gamma_{\rm b\overline{b}}$, $\Gamma_{\rm c\overline{c}}$ and $A_{FB}^{\rm c}$, are given in table 6. The dependence of these results on the Standard Model assumptions was discussed in section 5.6. The results after mixing correction are also quoted in this table.

The model dependence of the result is reduced by performing a two parameter fit for $A_{FB}^{\rm b,mix}$ and $A_{FB}^{\rm c}$. This was not done for the lower statistics off-peak data samples. The results for the on-peak data with $\langle\sqrt{s}\rangle = 91.24$ GeV are:

$$\begin{aligned} A_{FB}^{\rm b,mix} &= 0.070 \pm 0.014\,(\text{stat}) \pm 0.005\,(\text{sys}), \\ A_{FB}^{\rm b} &= 0.092 \pm 0.018\,(\text{stat}) \pm 0.007\,(\text{sys}) \pm 0.003\,(\text{mix}), \\ A_{FB}^{\rm c} &= 0.014 \pm 0.030\,(\text{stat}) \pm 0.020\,(\text{sys}). \end{aligned}$$

$\langle\sqrt{s}\rangle$(GeV)	A_{FB}^{c} (predicted)	$A_{FB}^{b,mix}$	A_{FB}^{b}
89.66	-0.029	$0.054 \pm 0.041 \pm 0.005$	$0.071 \pm 0.054 \pm 0.007 \pm 0.002$
91.24	0.056	$0.075 \pm 0.014 \pm 0.004$	$0.098 \pm 0.019 \pm 0.006 \pm 0.003$
92.75	0.111	$0.100 \pm 0.036 \pm 0.009$	$0.131 \pm 0.047 \pm 0.012 \pm 0.004$

Table 6: Results from one parameter fits for $A_{FB}^{b,mix}$. The Standard Model values of $\Gamma_{b\overline{b}}/\Gamma_{c\overline{c}}$ and A_{FB}^{c} are assumed. The first error is statistical and the second systematic. The third error, where quoted, is due to the uncertainty in χ.

The central values assume $\lambda = \Gamma_{c\overline{c}}/\Gamma_{b\overline{b}} = 0.171/0.217$, and the systematic error includes a 22% variation in λ. The values for the $b\overline{b}$ forward-backward asymmetry are in good agreement with the results of the one parameter measurements, with the advantage that the asymmetry of the $c \to \ell^+$ events is no longer constrained. This reduces the model dependence of the result, and the uncertainty in the value of A_{FB}^{c} is included in the statistical error on $A_{FB}^{b,mix}$.

The asymmetry values are compatible with those presented by other LEP Collaborations [25]. The results of the two parameter fit are compared with the Standard Model prediction in figure 10. The plot shows the one standard deviation curves in the A_{FB}^{b}–A_{FB}^{c} plane using electron data, muon data or both. All statistical and systematic errors are included. The Standard Model prediction is from the ZFITTER program [21], with $\sqrt{s} = 91.24$ GeV, $M_Z = 91.187$ GeV/c^2, a top mass in the range 50 to 250 GeV/c^2, a Higgs boson mass in the range 60 to 1000 GeV/c^2 and $0.11 < \alpha_s < 0.13$ [22]. The range of the prediction is dominated by the top mass uncertainty. The results are compatible with the Standard Model prediction, and have errors similar in size to the range of the prediction. The measurement of A_{FB}^{b} from the two parameter fit to the on-peak data sample, and those from the one parameter fits to the off-peak data samples are shown in figure 11. The curve is the prediction of ZFITTER, with $M_Z = 91.187$ GeV/c^2, $M_{top} = 132$ GeV/c^2, a Higgs boson mass of 300 GeV/c^2, and $\alpha_s = 0.12$. The results are in good agreement with the Standard Model prediction for all three values of $\langle\sqrt{s}\rangle$.

Acknowledgements

It is a pleasure to thank the SL Division for the efficient operation of the LEP accelerator, the precise information on the absolute energy, and their continuing close cooperation with our experimental group. In addition to the support staff at our own institutions we are pleased to acknowledge the
Department of Energy, USA,
National Science Foundation, USA,
Texas National Research Laboratory Commission, USA,
Science and Engineering Research Council, UK,
Natural Sciences and Engineering Research Council, Canada,
Fussefeld Foundation,
Israeli Ministry of Energy and Ministry of Science,
Minerva Gesellschaft,
Japanese Ministry of Education, Science and Culture (the Monbusho) and a grant under the Monbusho International Science Research Program,
German Israeli Bi-national Science Foundation (GIF),
Direction des Sciences de la Matière du Commissariat à l'Energie Atomique, France,
Bundesministerium für Forschung und Technologie, Germany,
National Research Council of Canada,
A.P. Sloan Foundation and Junta Nacional de Investigaccão Científica e Tecnológica, Portugal.

References

[1] *Z Physics at LEP 1 - Volume 1*, Edited by G. Altarelli, CERN 89-08, September 1989.

[2] OPAL Collaboration, Nucl. Instrum. Methods **A305** (1991) 275.

[3] M. Hauschild *et al.*, Nucl. Instrum. Methods **A314** (1992) 74.

[4] R. L. Gluckstern, Nucl. Instrum. Methods **24** (1963) 381.

[5] T. Sjöstrand, Comp. Phys. Comm. **39** (1986) 347;
T. Sjöstrand and M. Bengtsson, Comp. Phys. Comm. **43** (1987) 367;
T. Sjöstrand, CERN-TH.6488/92. OPAL optimised parameters were used, as described in OPAL Collaboration, Z. Phys. **C47** (1990) 505.

[6] J.Allison *et al.*, Nucl. Instrum. Methods **A317** (1992) 47.

[7] C.Peterson *et al.*, Phys. Rev. **D27** (1983) 105.

[8] ALEPH Collaboration, Phys. Lett. **B244** (1990) 551;
DELPHI Collaboration, Z. Phys. **C56** (1992) 47;
L3 Collaboration, Phys. Lett. **B261** (1991) 177;
OPAL Collaboration, Phys. Lett. **B263** (1991) 311;
ALEPH Collaboration, Phys. Lett. **B266** (1991) 218.

[9] OPAL Collaboration, Phys. Lett. **B262** (1991) 341.

[10] OPAL Collaboration, Z. Phys. **C52** (1991) 175.

[11] JADE Collaboration, Z. Phys. **C33** (1986) 23;
JADE Collaboration, Phys. Lett. **B213** (1988) 235.

[12] OPAL Collaboration, Z. Phys. **C49** (1991) 375.

[13] OPAL Collaboration, CERN-PPE/93-46, March 1993, to be published in Z. Phys. **C**.

[14] OPAL Collaboration, Z. Phys. **C55** (1992) 191.

[15] CLEO Collaboration, S.Henderson *et al.*, Phys. Rev. **D 45** (1992) 2212;
M.Worris, Thesis, Cornell University, 1991 (unpublished).

[16] G.Altarelli *et al.*, Nucl. Phys. **B 208** (1982) 365.

[17] N.Isgur, D.Scora, B.Grinstein and M.Wise, Phys. Rev. **D39** (1989) 799.

[18] C. Quigg and J. L. Rosner, Phys. Rev. **D19** (1979) 1532.
The masses assumed were 5.0 ± 0.3 GeV/c^2 for the bottom quark, 1.5 ± 0.2 GeV/c^2 for the charm quark and 1.78 GeV/c^2 for the τ.

[19] Particle Data Group, Phys. Rev. **D45** (1992).

[20] DELCO Collaboration, W.Bacino *et al.*, Phys. Rev. Lett. **43** (1979) 1073.

[21] D. Bardin *et al.*, CERN-TH 6443/92, May 1992.

[22] The Working Group on Lep Energy and the LEP collaborations ALEPH, DELPHI, L3 and OPAL, CERN-PPE/93-53, March 1993, subm. to Phys Lett. B;
The LEP Collaborations, ALEPH, DELPHI, L3 and OPAL, Phys. Lett. **B276** (1992) 247.

[23] OPAL Collaboration, Phys. Lett. **B294** (1992) 436.

[24] *Electroweak b physics at LEP*, presented by R. Tenchini at the XXVIIIth Rencontre de Moriond, Les Arcs, France, March 1993.

[25] ALEPH Collaboration, Phys. Lett. **B263** (1991) 325;
DELPHI Collaboration, Phys. Lett. **B276** (1992) 536;
L3 Collaboration, Phys. Lett. **B292** (1992) 454.

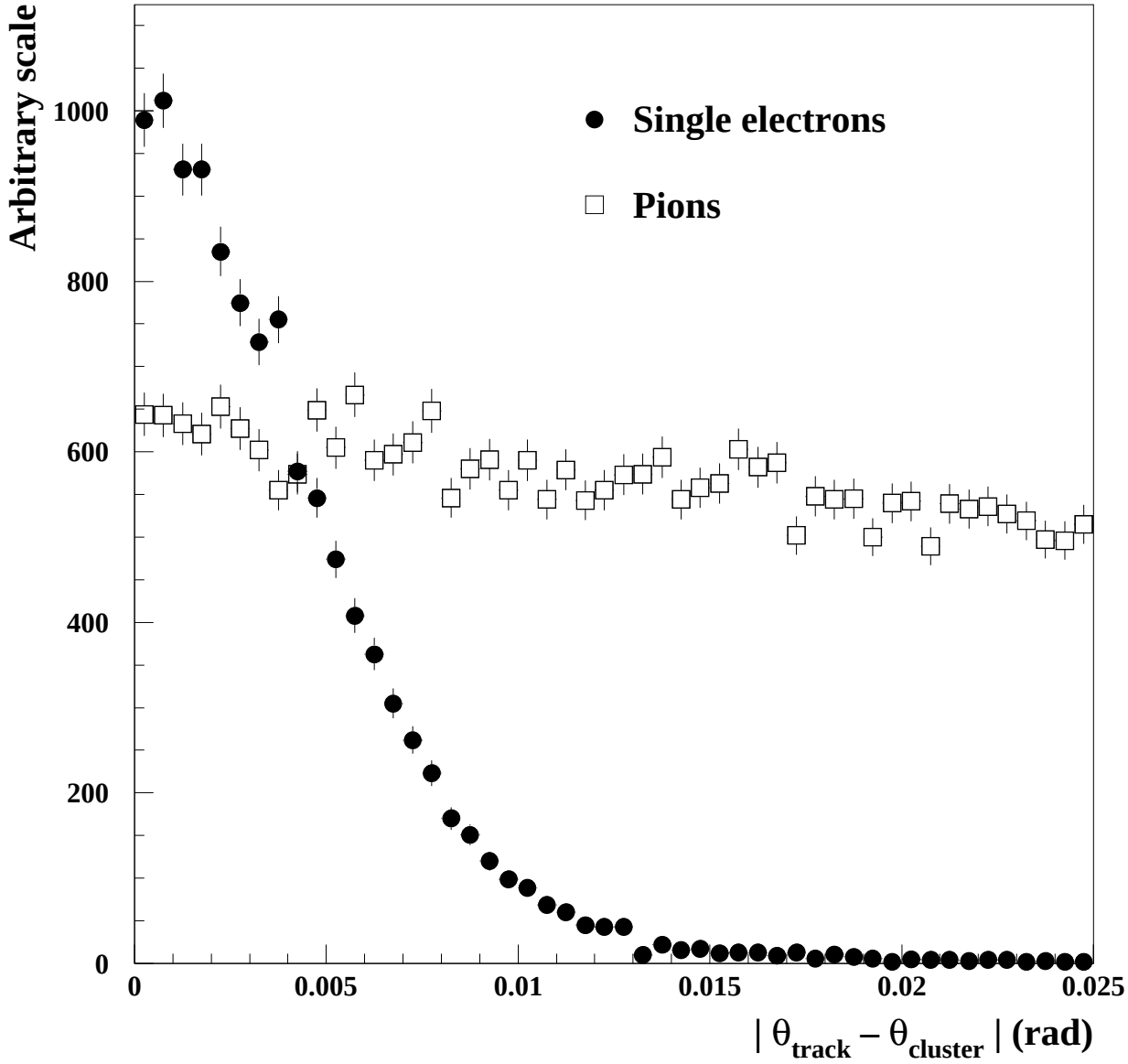

Figure 1: The distribution of $|\theta_{\rm track} - \theta_{\rm cluster}|$ for electrons in low multiplicity events and pions from K^0 decays. The electron selection cut is at 8 mrad.

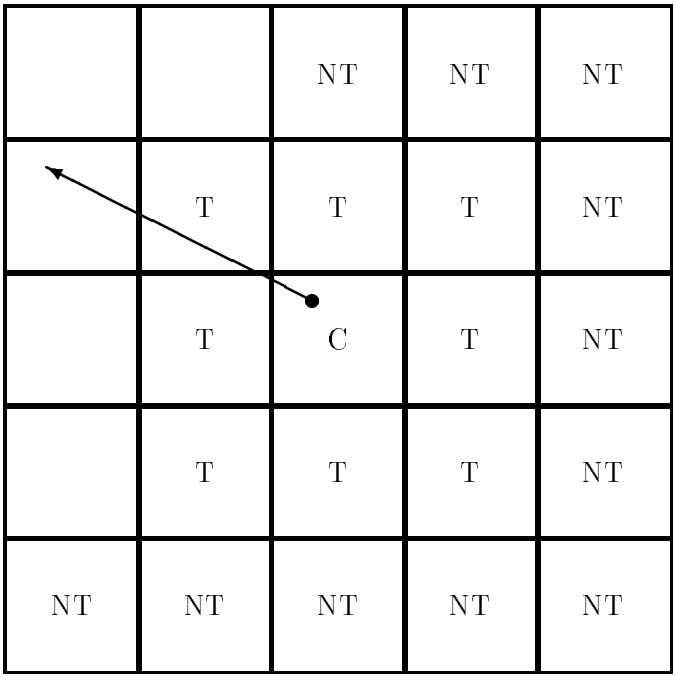

Figure 2: The geometry used for the background subtracted energy. The track impact point is denoted by •, with a momentum vector in the x–y plane as indicated. C denotes the centre block. Blocks denoted T are the touching blocks and NT denotes the next-to-touching blocks used in the background calculation.

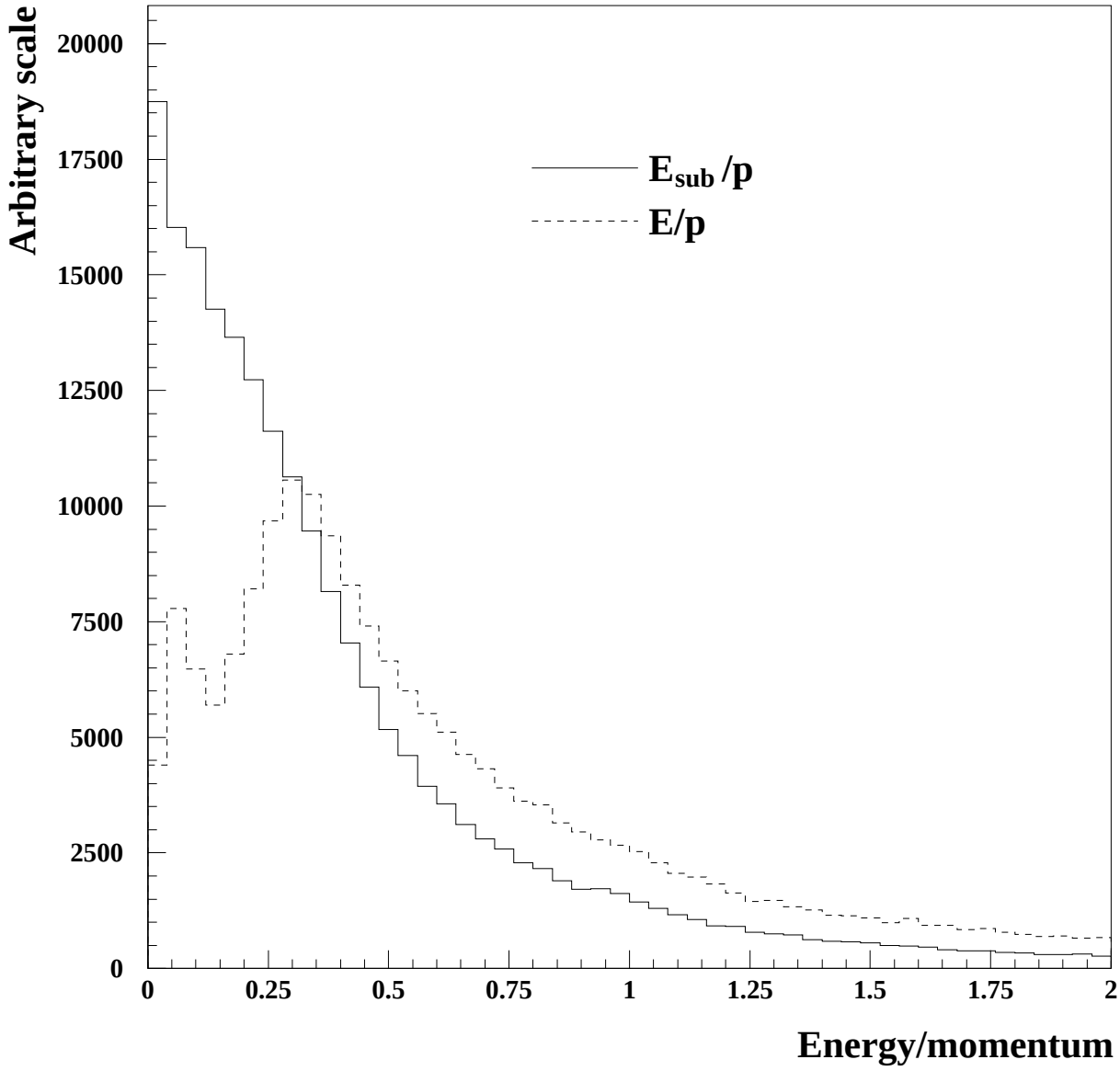

Figure 3: The background subtracted energy–momentum ratio, $E_{\rm sub}/p$, compared to the ratio of the cluster energy to momentum, E/p, for pions from K^0 decays. In the signal region ($0.8 < E_{\rm sub}/p < 1.2$), the modified energy estimate provides a reduced background.

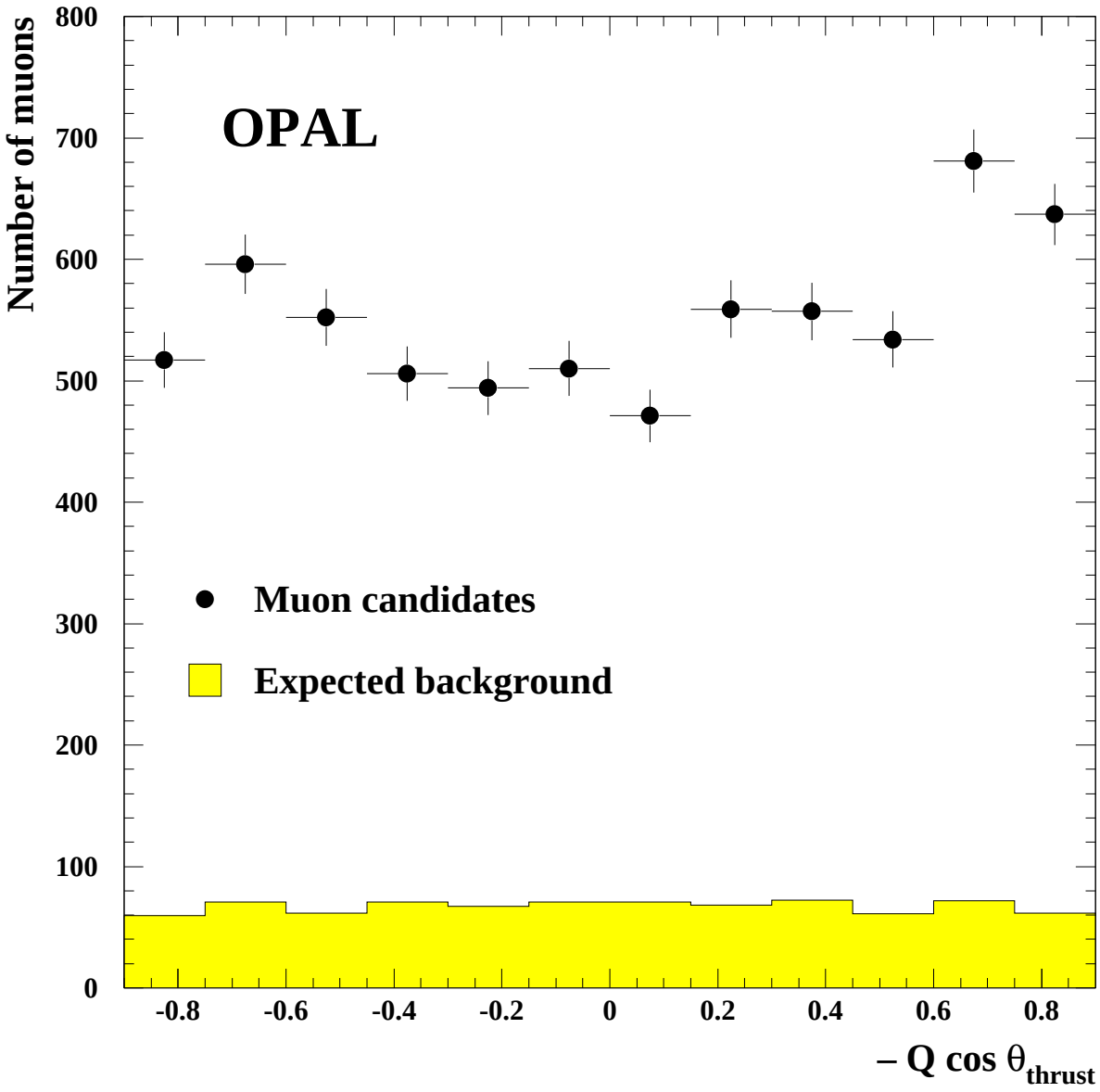

Figure 4: The distribution of $y = -Q\cos\theta_{\rm thrust}$ for all muon candidates with $p > 3$ GeV/c and $p_t > 1$ GeV/c. The shaded area indicates the predicted hadronic background.

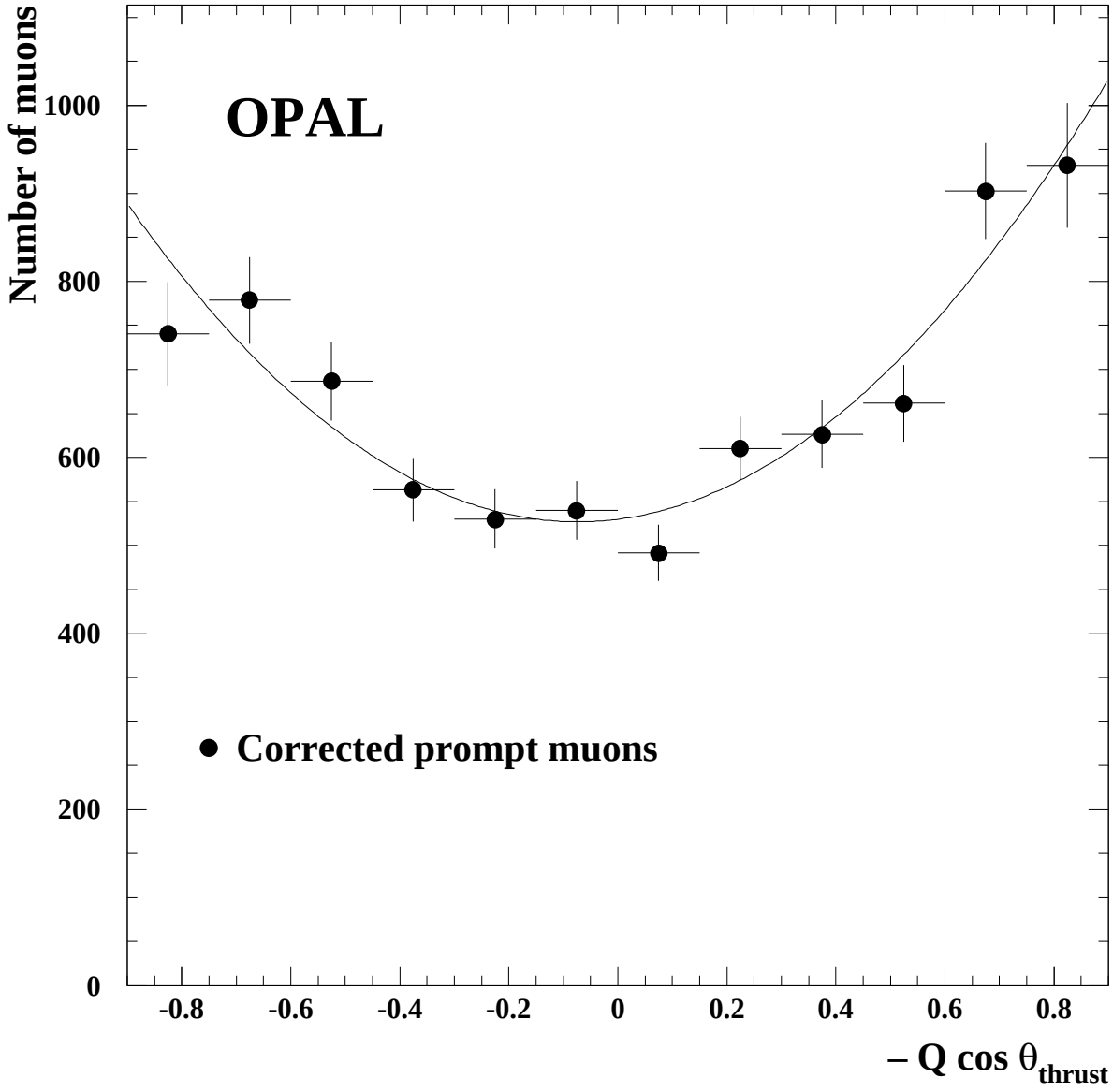

Figure 5: The distribution of $y = -Q\cos\theta_{\rm thrust}$ for prompt muons with $p > 3$ GeV/c and $p_t > 1$ GeV/c, after subtraction of the predicted background and correcting for efficiency. The curve shows the result of the χ^2 fit.

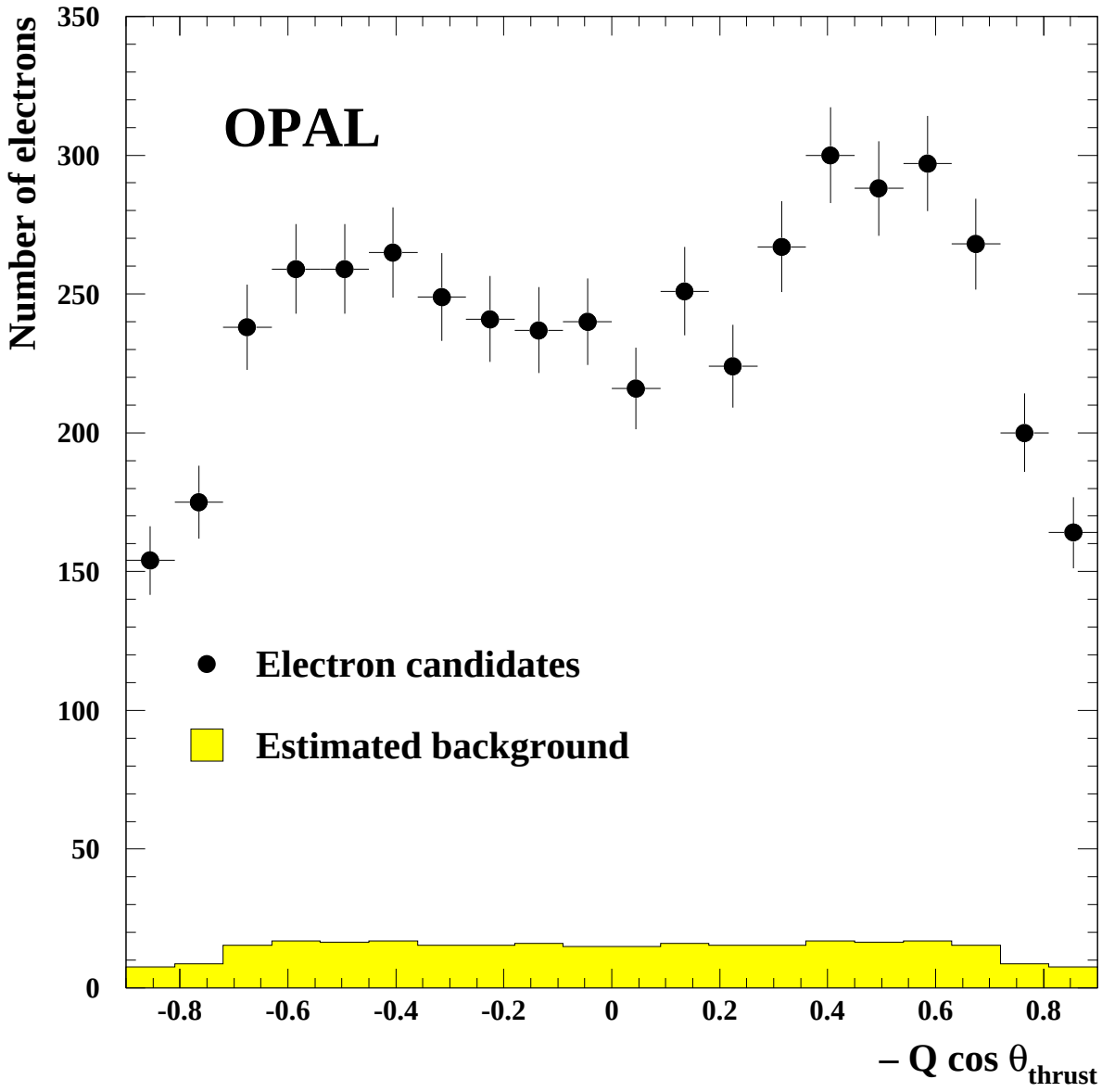

Figure 6: The distribution of $y = -Q\cos\theta_{\rm thrust}$ for all electron candidates with $p > 2$ GeV/c and $p_t > 0.8$ GeV/c.

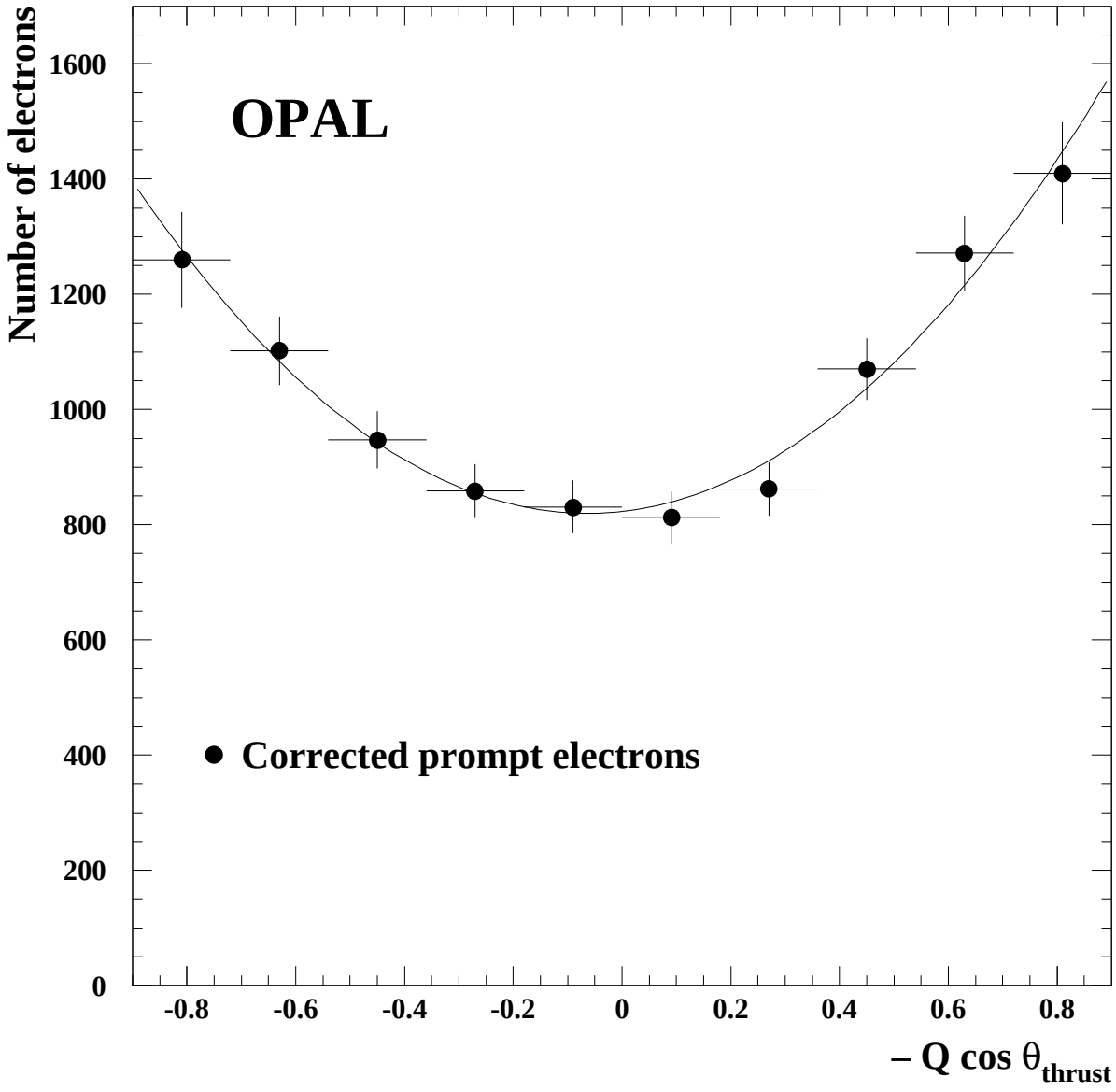

Figure 7: The distribution of $y = -Q\cos\theta_{\rm thrust}$ for electron candidates with $p > 2$ GeV/c and $p_t > 0.8$ GeV/c, after subtracting non-prompt backgrounds, and correcting for efficiency. The result of an event-by-event likelihood fit to the uncorrected data to measure the effective asymmetry is superimposed.

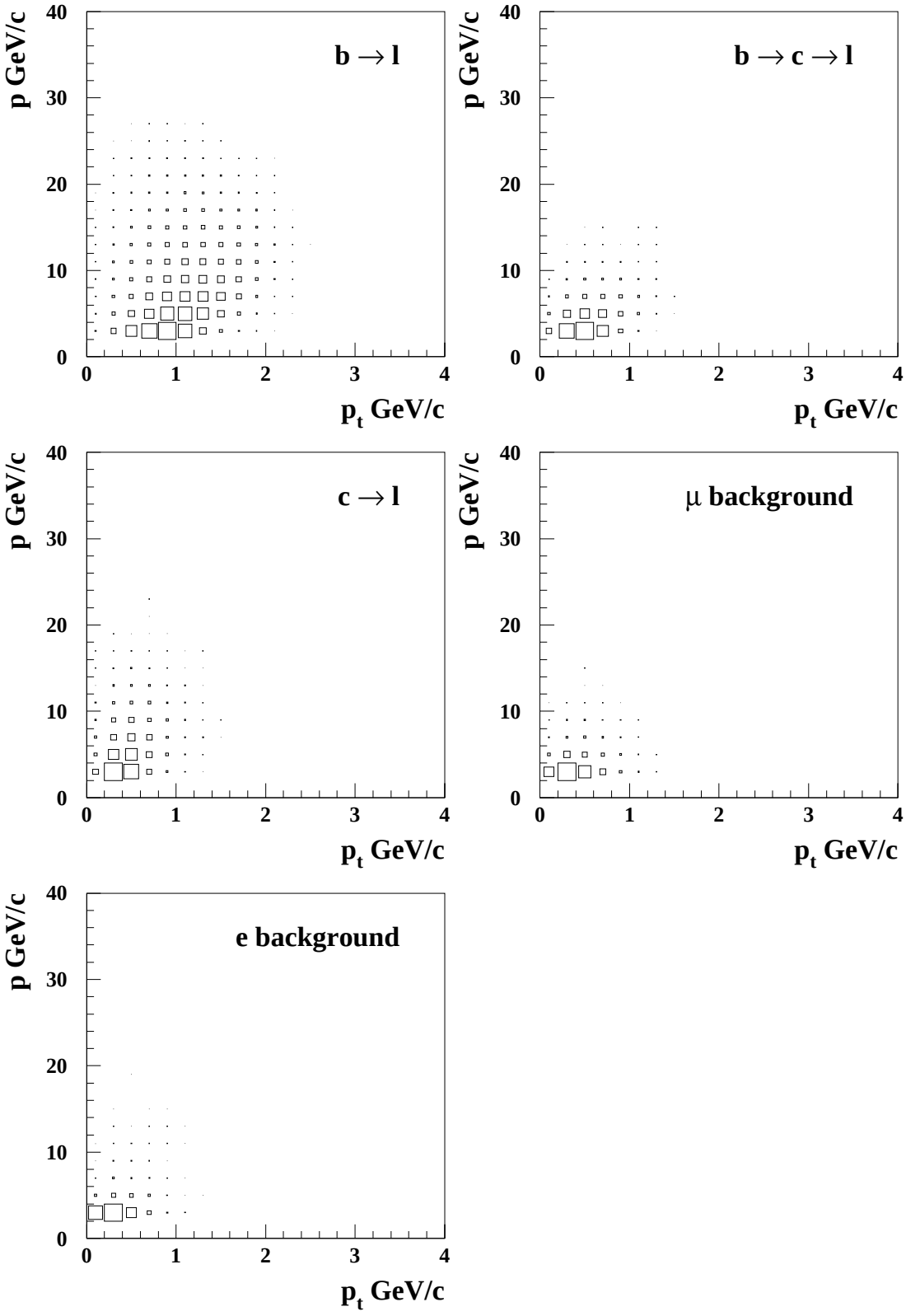

Figure 8: The p–p_t distributions of leptons from different sources. The area of each square is proportional to the number of events in that region. The overall normalisation of each source is arbitrary.

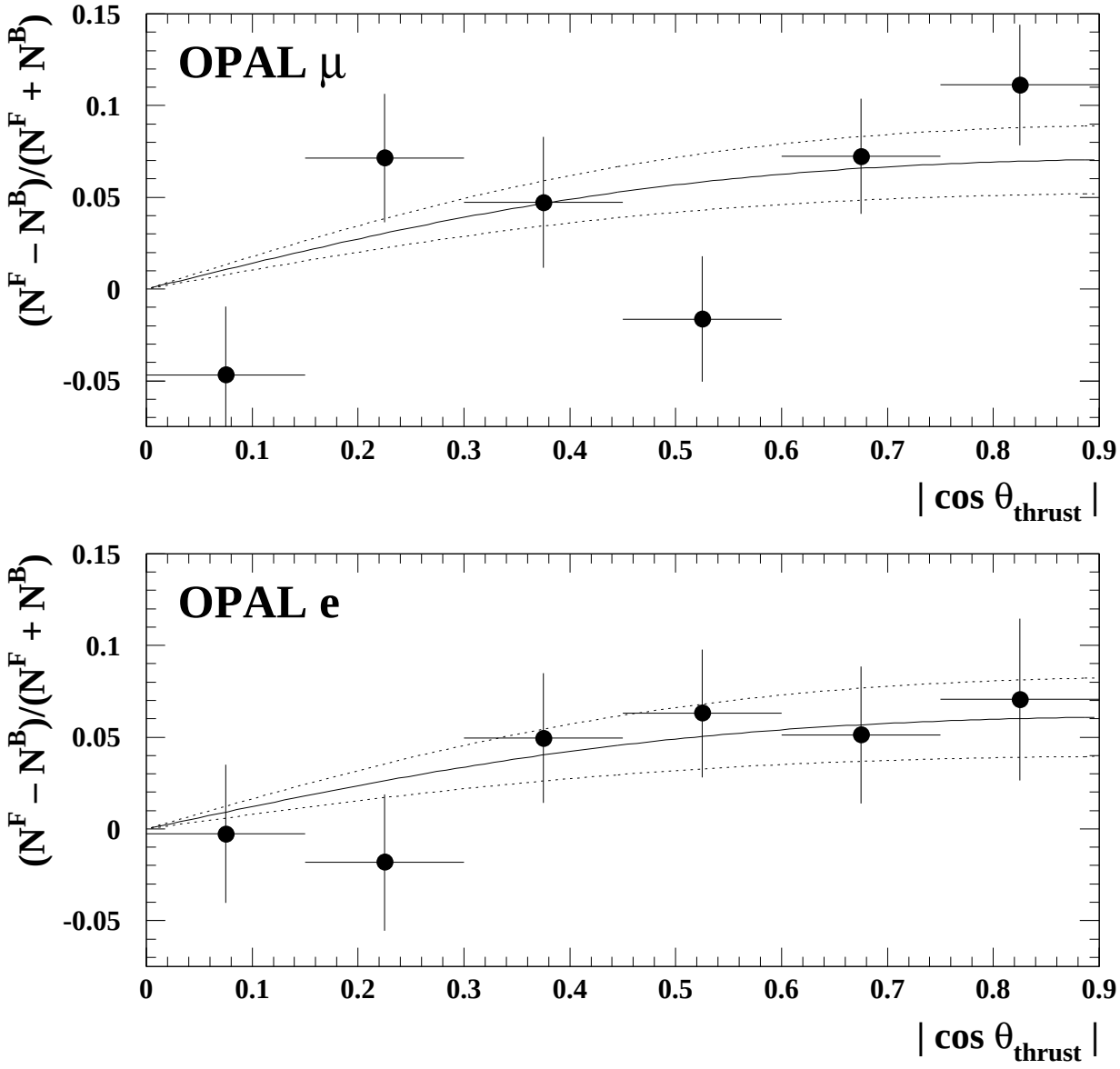

Figure 9: The ratio $(N^F - N^B)/(N^F + N^B)$ vs. $|y| = |\cos\theta_{\rm thrust}|$, for prompt muons with $p > 3$ GeV/c and $p_t > 1$ GeV/c, and prompt electrons with $p > 2$ GeV/c and $p_t > 0.8$ GeV/c. The curves are of the form $8A_{FB}^{\rm obs}|y|/3(1+y^2)$. The solid curves are for the fitted values of $A_{FB}^{\rm obs}$, and the dotted curves are for values of $A_{FB}^{\rm obs}$ one standard deviation from the fitted values.

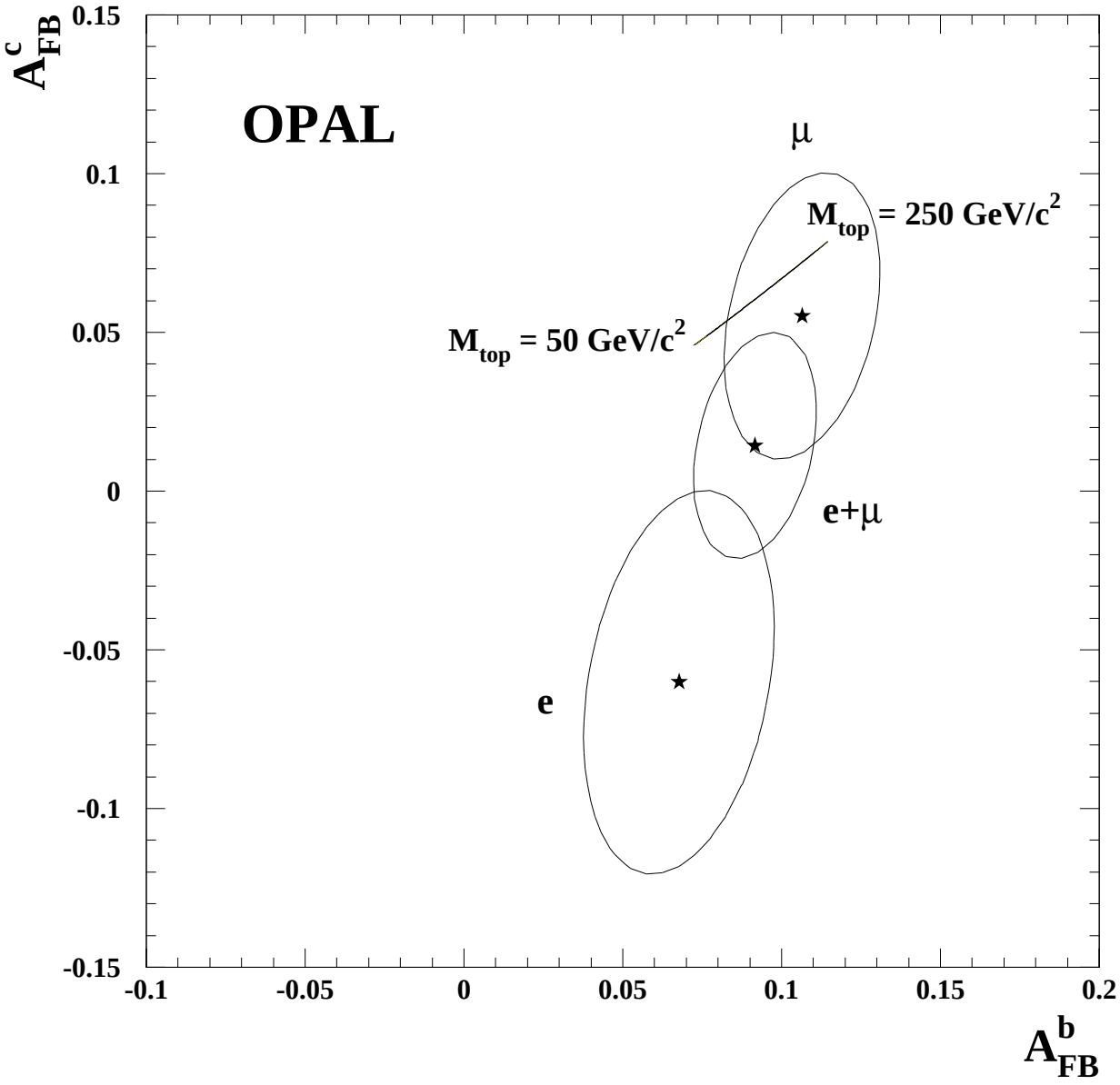

Figure 10: One standard deviation contours (39% probability content) for the results of the two parameter fit to data with electron candidates, muon candidates or both. The line indicates the Standard Model prediction, for which the dominant uncertainty is from the range of top quark mass.

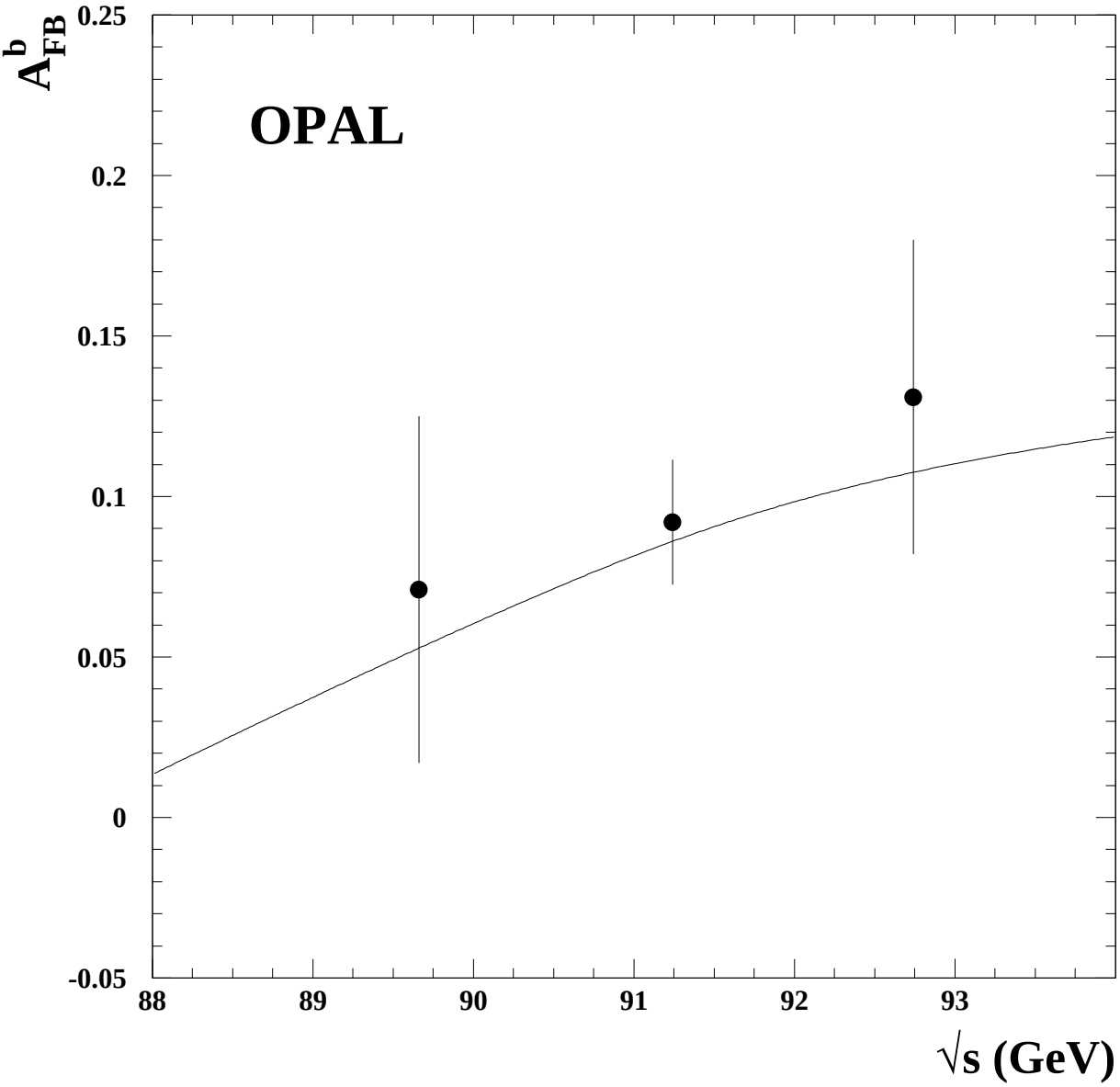

Figure 11: The results for A_{FB}^{b} as a function of centre-of-mass energy. The curve is the Standard Model prediction.